The protein kinase LKB1 promotes self-renewal and blocks invasiveness in glioblastoma

Caja, L.; Dadras, M.S.; Mezheyeuski, A.; Rodrigues-Junior, D.M.; Liu, S.J.; Webb, A.T.; ... ; Moustakas, A.

Received: 22 May 2021 | Revised: 10 July 2021 | Accepted: 24 July 2021

DOI: 10.1002/jcp.30542

RESEARCH ARTICLE

Journal of Cellular Physiology WILEY

The protein kinase LKB1 promotes self-renewal and blocks invasiveness in glioblastoma

Laia Caja[1] | Mahsa Shahidi Dadras[1,2] | Artur Mezheyeuski[2] | Dorival Mendes Rodrigues-Junior[1] | Sijia Liu[3] | Anna Taylor Webb[1,4] | Maria Catalina Gomez-Puerto[3] | Peter ten Dijke[3] | Carl-Henrik Heldin[1] | Aristidis Moustakas[1]

[1]Department of Medical Biochemistry and Microbiology and Ludwig Institute for Cancer Research, Science for Life Laboratory, Biomedical Center, Uppsala University, Uppsala, Sweden

[2]Department of Immunology, Genetics and Pathology, Rudbeck Laboratory, Science for Life Laboratory, Uppsala University, Uppsala, Sweden

[3]Department of Cell and Chemical Biology, Oncode Institute, Leiden University Medical Center, Leiden, The Netherlands

[4]Department of Cell and Molecular Biology, Karolinska Institutet, Stockholm, Sweden

Correspondence

Aristidis Moustakas, Department of Medical Biochemistry and Microbiology and Ludwig Institute for Cancer Research, Science for Life Laboratory, Box 582, Biomedical Center, Uppsala University, SE-751 23 Uppsala, Sweden.
Email: aris.moustakas@imbim.uu.se

Funding information

H2020 European Research Council, Grant/Award Number: 787472; Vetenskapsrådet, Grant/Award Numbers: 2014-3834, 2015-02757, 2017-01588, 2018-02757, 2020-01291; Ludwig Institute for Cancer Research, Grant/Award Number: Uppsala Branch; OE och Elda Johanssons stiftelse, Grant/Award Numbers: 2018, 2019; Petrus och Augusta Hedlunds Stiftelse, Grant/Award Number: M2019-1065; Magnus Bergvalls Stiftelse, Grant/Award Number: 2019-03444; Cancerfonden,

Abstract

The role of liver kinase B1 (LKB1) in glioblastoma (GBM) development remains poorly understood. LKB1 may regulate GBM cell metabolism and has been suggested to promote glioma invasiveness. After analyzing LKB1 expression in GBM patient mRNA databases and in tumor tissue via multiparametric immunohistochemistry, we observed that LKB1 was localized and enriched in GBM tumor cells that co-expressed SOX2 and NESTIN stemness markers. Thus, LKB1-specific immunohistochemistry can potentially reveal subpopulations of stem-like cells, advancing GBM patient molecular pathology. We further analyzed the functions of LKB1 in patient-derived GBM cultures under defined serum-free conditions. Silencing of endogenous LKB1 impaired 3D-gliomasphere frequency and promoted GBM cell invasion in vitro and in the zebrafish collagenous tail after extravasation of circulating GBM cells. Moreover, loss of LKB1 function revealed mitochondrial dysfunction resulting in decreased ATP levels. Treatment with the clinically used drug metformin impaired 3D-gliomasphere formation and enhanced cytotoxicity induced by temozolomide, the primary chemotherapeutic drug against GBM. The IC_{50} of temozolomide in the GBM cultures was significantly decreased in the presence of metformin. This combinatorial effect was further enhanced after LKB1 silencing, which at least partially, was due to increased apoptosis. The expression of genes involved in the maintenance of tumor stemness, such as growth factors and their receptors, including members of the platelet-derived growth factor (PDGF) family, was suppressed after LKB1 silencing. The defect in gliomasphere growth caused by LKB1 silencing was bypassed after supplementing the cells with exogenous PFDGF-BB. Our data support the parallel roles of LKB1 in maintaining mitochondrial homeostasis, 3D-gliomasphere survival, and hindering migration in GBM.

Laia Caja and Mahsa Shahidi Dadras contributed equally to this study.

Grant/Award Numbers: CAN 2015/438, CAN2018/469; Svenska Läkaresällskapet, Grant/Award Number: SLS-887701; Lisa Erikssons minnesfond, Grant/Award Number: 2013

Thus, the natural loss of, or pharmacological interference with LKB1 function, may be associated with benefits in patient survival but could result in tumor spread.

KEYWORDS
cancer stem cells, glioblastoma, invasion, LKB1, metformin

1 | INTRODUCTION

Glioblastoma (GBM) or grade IV glioma is an invasive and lethal primary brain tumor with a median patient survival of about one year after diagnosis (Alcantara Llaguno et al., 2016; Lathia et al., 2015). Gene copy number, methylation and expression analyses classify GBM into proneural (PN), classical (CL), and mesenchymal (MS) subtypes (McLendon et al., 2008; Noushmehr et al., 2010; Verhaak et al., 2010; Q. Wang, Hu, et al., 2017). Recent work emphasizes the functional role of GBM stem-like cells (Singh et al., 2004), resisting radiation or chemotherapy and causing tumor recurrence (Bao et al., 2006; Chen et al., 2012). Signaling pathways that regulate neural/glial stem cells during development and adult homeostasis, including platelet-derived growth factor (PDGF), transforming growth factor-β (TGF-β), leukemia inhibitory factor (LIF), Wnt, epidermal growth factor (EGF) and Notch, also regulate the GBM stem-like cells. These signaling pathways regulate the expression of transcription factors, such as NANOG, MYC, OLIG2, SALL2, SOX2, and POUF3, which control GBM stem-like cell survival and propagation (Lathia et al., 2015).

The *Liver Kinase B1* (*LKB1*, alias *STK11*) gene is mutated in sporadic lung adenocarcinomas, cervical cancers, and in gastrointestinal polyps of Peutz-Jeghers syndrome patients (Korsse et al., 2013; Vaahtomeri & Mäkelä, 2011). LKB1 is a serine/threonine kinase forming a catalytically active trimer with the pseudokinase STRAD and the scaffold protein MO25/CAB39 that phosphorylates downstream serine/threonine kinases of the AMP-regulated protein kinase (AMPK) family (Korsse et al., 2013; Vaahtomeri & Mäkelä, 2011). LKB1/STRAD/MO25 signaling arrests the cell cycle, induces cell death, regulates cell polarity including mitotic spindle orientation and regulates metabolism (Korsse et al., 2013; Vaahtomeri & Mäkelä, 2011). In normal hematopoietic and leukemic stem cells, signaling by LKB1 regulates cell cycle and metabolism, contributing to the maintenance of stemness (Gan et al., 2010; Gurumurthy et al., 2010; Nakada et al., 2010).

The relevance of LKB1 function in GBM remains less studied; 23.6% of GBM patients exhibit loss of heterozygosity at the 19p13.3 region encompassing the *LKB1/STK11* locus (Sobottka et al., 2000), without specific mutations in the LKB1 protein (Ritland et al., 1995). Certain high-grade human gliomas express low LKB1 levels (Huang et al., 2017). On the other hand, micro-RNA *miR-451* downregulates the scaffolding partner MO25/CAB39, promoting proliferation and suppressing GBM cell migration (Godlewski et al., 2010; Kim et al., 2011; Schuetz et al., 2012; Zhao et al., 2017). To elucidate the functions of LKB1 in GBM, we analyzed its expression in situ by multiparametric immunohistochemistry and silenced LKB1 in patient-derived GBM cultures. We have uncovered links between LKB1 and different aspects of GBM cell biology, i.e. the growth of gliomaspheres, invasiveness, drug resistance, as well as mitochondrial activity, and ATP production.

2 | MATERIALS AND METHODS

2.1 | Patient-derived GBM cell culture

GBM cultures were gifts from the human GBM cell culture resource, which collects and authenticates primary cells isolated from grade IV glioma biopsies (https://www.hgcc.se/). Ethical protocols and permission have been secured by the biobank (Xie et al., 2015). Cells were cultured on laminin (Sigma-Aldrich Sweden AB), in Dulbecco's modified Eagle's medium (DMEM)/F12 Glutamax and Neurobasal medium (both from Life Technologies Europe BV) mixed at a 1:1 ratio, with the addition of B27 and N2 supplements (both from Life Technologies), penicillin/streptomycin (Sigma-Aldrich Sweden AB), 10 ng/ml EGF and fibroblast growth factor 2 (FGF2) (PeproTech EC Ltd). Cells were dissociated with accutase and used between passages 15–25.

2.2 | Tissue microarray (TMA) analysis

We analyzed a TMA that contained 35 independent GBM patient samples and 5 normal brain tissue samples, each in duplicate, generating 80 tissue cores per TMA (GL806d; US Biomax). Multiplexed immunohistochemical protocols (Mezheyeuski et al., 2018) were adapted as follows. TMA slides were deparaffinized in xylene, hydrated in graded alcohols, and fixed in neutral buffered formalin for 20 min. For antigen retrieval, slides were microwaved in pH 9.0 buffer (AR6001, PerkinElmer Sverige AB) for 15 min. The primary antibodies, mouse anti-LKB1/STK11 (Santa Cruz Biotechnology Inc.), anti-GFAP (Santa Cruz Biotechnology), anti-SOX2 (Millipore/Merck), and rabbit anti-NESTIN (Millipore/Merck), were diluted (1:50) in ready-to-use diluent and blocking buffer (ARD1001EA, PerkinElmer Sverige AB). Slides were incubated for 30 min at room temperature, followed by incubation with anti-rabbit/mouse Opal Polymer HRP ready-to-use immunohistochemistry detection reagent (ARH1001EA, PerkinElmer Sverige AB) for 10 min at room temperature. Following washing, slides were developed for 10 min using Opal 520/540/570/690 (FP1488001KT, FP1496001KT, PerkinElmer) fluorophores for visualization of LKB1, SOX2, NESTIN, and GFAP, respectively, before nuclear staining with 4′,6-diamidino-2-phenylindole (DAPI) and mounting with ProlongTM Diamond Antifade (Thermo Fisher Scientific). After the first staining, primary/secondary antibodies were

removed by boiling, followed by staining for the next antigen, and repeated in total four times.

Using the Vectra Polaris system (Akoya Biosciences) multispectral imaging mode, TMAs were scanned (×20 magnification), and images were analyzed with the Inform software by applying spectral unmixing and cell segmentation. Mean expression levels of each antigen in every cell region were recorded. Intensity thresholds that separated specific signals from the background were defined by visual evaluation. Furthermore, potential fluorescent signal leakage was estimated as explained in supplementary file 1. Data analysis was performed by R, version 3.3.3 (R Core Team, 2017; Team R., 2015). Cells were split into two classes, $SOX2^{high}/NESTIN^{high}/GFAP^{low}$ (GBM_Stem) and $SOX2^{low}/NESTIN^{low}/GFAP^{high}$ (GBM_diff), according to the expression levels of stemness (SOX2 and NESTIN) and astrocytic (GFAP) markers. LKB1 intensity was normalized by setting the background threshold to "zero" intensity and excluding cells with LKB1 signal below the background threshold. Thus, 3027 cells were $SOX2^{low}/NESTIN^{low}/GFAP^{high}$ in non-tumoral brain sections, 2882 cells in GBM sections, and 236 cells were $SOX2^{high}/NESTIN^{high}/GFAP^{low}$, detected only in GBM sections. Statistical difference between LKB1 levels in different cell subgroups was calculated by the Wilcoxon signed-rank test for two samples, which is equivalent to the Mann-Whitney *U*-rank test.

2.3 | Correlation analysis of gene expression

For Pearson correlation analysis of expression of specific genes ($R > 0.3$, p value < 0.05), the Gliovis data portal (Bowman et al., 2017) was used to analyze GBM samples from TCGA (Brennan et al., 2013; McLendon et al., 2008), included in the U133A, Agilent-4502A, and RNAseq experiments, and from Gravendeel (Gravendeel et al., 2009), included in the U133plus2 experiment.

2.4 | Short interfering (si) RNA transfection

Cells transfected at 80% confluence using siLenfect (Bio-Rad Laboratories AB) and siRNA (20 nM), according to the manufacturer (Dharmacon/GE Healthcare) for 24 h, were dissociated with accutase and seeded for experiments. The human-specific siRNA oligonucleotides were: ON-TARGETplus-Nontargeting-Pool (D-001810-10); ON-TARGETplus-Human-STK11(6794)-siRNA-SMARTpool and a set of 4 upgrades (L-005035-00, LU-005035-00).

2.5 | Zebrafish tail invasion experiment

Staging and embryo production of Tg(*Fli1:EGFP*) zebrafish were conducted as described (Ren et al., 2017). Cells stained with 4 ng/µl CM-DiI Dye (Thermo Fisher Scientific) were incubated for 4 min at 37°C followed by 15 min at 4°C, centrifuged for 5 min at 1200 rpm and resuspended in media, centrifuged again, and washed twice with phosphate-buffered saline (PBS); single-cell suspensions were stored in PBS at 4°C until implantation. Cell suspensions loaded into borosilicate glass capillary needles (1 mm O.D. × 0.78 mm I.D., Harvard Apparatus) were injected into embryos using a Pneumatic Picopump and a manipulator (WPI). Embryos were dechorionized 2 days post fertilization, anesthetized with 0.003% tricaine (Sigma-Aldrich), mounted on a 10-cm Petri dish coated with 1% agarose gel, and 400 cells were injected in the duct of Cuvier. Implanted embryos were maintained at 33°C, fixed in 4% paraformaldehyde for 2 h at room temperature, and imaged in PBS with 0.1% Tween-20 (Millipore/Merck), with a Leica SP5 STED confocal microscope (Leica). Both total number of fluorescent cells per injected fish and fluorescent cell extravasated from the tail fin vasculature and invading the fin were recorded.

2.6 | RNA expression analysis

RNA from ~250,000 cells was purified (Nucleospin Kit, Macherey-Nagel), 1 µg RNA was reverse-transcribed using the High-Capacity cDNA Reverse Transcription Kit (Thermo Fisher Scientific), followed by real-time PCR performed as described (Caja et al., 2018), with primers: *hsGAPDH* Fwd-GGAGTCAACGGATTTGGTCGTA, Rev-GGCAACAATATCCACTTTACCA; *hsLKB1/STK11* Fwd-TGACATCATCTACACTCAGGACTTCA, Rev-CCTCTGTGCCGTTCATACACA; *hsOLIG2* Fwd-CTTCAAGTCATCCTCGTCCAG, Rev-TGTTGATCTTGAGACGCAGC; *hsNESTIN* Fwd-AGCCCTGACCACTCCAGTTTAG, Rev-CCCTCTATGGCTGTTTCTTTCTCT; *hsGFAP* Fwd-TGCGGCTCGATCAACTCA, Rev-GTTGGTTTCATCCTGGAGCTTCT.

RNAseq was performed using the Ion Proton System (Life Technologies). Triplicate RNA samples per condition were reverse-transcribed using the Ion AmpliSeq Transcriptome Human Gene Expression kit (Revision A.0), according to the manufacturer (Life Technologies). Sequence reads were analyzed by AmpliSeqRNA analysis plugin, v4.2.1, in the Torrent Suite Software (Life Technologies), counting the number of sequences obtained for all cDNA amplicons. The resulting counts represent gene expression levels for over 20,800 genes, which were merged into a table, used for differential expression analysis with standard parameters of the R/Bioconductor package EdgeR (http://www.bioconductor.org/) (Robinson et al., 2010). Benjamini-Hochberg analysis estimated the false discovery rate (FDR) and adjusted p-values (padj) for multiple testing estimated the significance of differential expression. Functional enrichment of differentially expressed genes was based on the R package clusterProfiler (http://www.bioconductor.org/) (Yu et al., 2012). Primary data deposited to Array Express (accession number E-MTAB-7724) are presented in File S2.

2.7 | Immunoblotting

Proteins from ~600,000 cells were extracted in 0.5% Triton X-100, 0.5% Na-deoxycolate, 20 mM Tris, pH 7.4, 150 mM NaCl, 10 mM

EDTA, complete protease inhibitor cocktail (Roche Diagnostics Scandinavia AB) for 30 min on ice, and centrifuged at 13,000 rpm for 10 min at 4°C to remove insoluble debris. Proteins subjected to SDS polyacrylamide gel electrophoresis were immunoblotted with mouse anti-LKB1, rabbit anti-AMPKα, anti-pAMPKα, anti-p62, anti-LC3B, and anti-caspase-3 antibodies (Cell Signaling Technology); blotting with mouse anti-GAPDH (Thermo Fisher Scientific) or anti-β-ACTIN (Santa Cruz Biotechnology) were used as loading controls. The specificity of detected proteins was verified in multiple cell models, based on ascribed electrophoretic mobility and by loss or significant decrease of protein signal upon silencing of the protein. Densitometric quantification was performed using ImageJ (NIH) software. The digital density of protein bands was measured as a differential from their surrounding "empty" area and was normalized against the corresponding loading control. Density under basal or control conditions appears as 1. LKB1 expression levels in different immunoblots generated from the same GBM culture reproducibly gave almost the same protein band intensity, which is represented by a value of 1 in the figures. Original immunoblots are in Figures S10–S13.

2.8 | Invasion assays

Transwell inserts (Corning) for 24-well plates (6.5 mm diameter, 8 µm pore) were coated with 10 µg/ml laminin (Sigma-Aldrich) and incubated at 37°C for 1 h. Cells (5×10^4) were seeded in serum-free DMEM in the upper chamber, and DMEM/6% FBS was placed in the lower chamber. After 16 h, non-migrating cells were removed with a cotton swab, and inserts were fixed in methanol and stained with DAPI. Nuclei were counted in 10–15 pictures of each insert, taken at ×20 magnification, using ImageJ.

2.9 | Sphere and extreme limiting dilution assays (ELDA)

Single-cell suspensions were seeded at 1000 cells/well in 24-well plates and spheres larger than 50 µm in diameter were recorded after 7 days. Decreasing numbers, 64-1 cells/well, grew in low-attachment 96-well plates in 200 µl stem cell media (i) with or without PDGF-BB (25 ng/ml), or (ii) with or without metformin (5 mM; Sigma-Aldrich). Each dilution included 6 or 7 replicates per experiment. On Day 7, wells containing spheres were scored for each plating density and analyzed by the ELDA software (http://bioinf.wehi.edu.au/software/elda), which estimates a stem cell frequency per condition (Hu & Smyth, 2009). Data are plotted as log-fraction of wells without spheres as a function of the plated cell number.

2.10 | Intracellular redox analysis

After transfection, 80,000 cells/well seeded in 12-well plates were subjected to intracellular redox measurement 1 day after seeding. Cells were incubated with the oxidation-sensitive fluorescent probes (Thermo Fisher Scientific) 2′,7′-dichlorodihydrofluorescein diacetate (H_2DCFDA, 2.5 µM, 30 min, 37°C) and MitoSOX™ Red (5 µM, 10 min, 37°C) in Hank's balanced salt solution (HBSS) without phenol red, and then cells were lysed in 25 mM HEPES, pH 7.5, 60 mM NaCl, 1.5 mM $MgCl_2$, 0.2 mM EDTA, 0.1% Triton X-100 (10 min, 4°C) and transferred in duplicate into a 96-well plate, where fluorescence was measured (H_2DCFDA Ex/Em 495/520 nm; MitoSOX™ Red Ex/Em 510/580 nm) in a microplate reader Enspire (PerkinElmer). H_2DCFDA and MitoSOX™ Red measured total intracellular reactive oxygen species (ROS) content and mitochondrial superoxide production, respectively, which were expressed as percentages relative to control after correction for protein content, determined using Bradford Reagent (Bio-Rad).

2.11 | Mitochondrial transmembrane potential analysis

After transfection, 125,000 cells/well seeded in six-well plates were analyzed after 2 days. The fluorescent probes MitoTracker™, Red CMXRos (Thermo Fisher Scientific) were used to fluorimetrically analyze the mitochondrial transmembrane potential and mitochondrial mass, respectively. Cells incubated with 500 nM final probe concentration in HBSS without phenol red for 30 min at 37°C, were detached by accutase, resuspended in 250 µl of the same media, 100 µl of which was transferred in duplicate into a 96-well plate for fluorescence recording (MitoTracker™ Red CMXRos Ex/Em 579/599 nm) in the microplate reader Enspire. Data are expressed as a percentage of control after correction for protein content, determined using Bradford Reagent (Bio-Rad).

2.12 | Intracellular ATP analysis

Three days after transfection, 125,000 cells/well seeded in six-well plates were scraped, centrifuged at 2500 rpm at 4°C, lysed in H_2O, and boiled for 5 min, before ATP Determination Kit analysis (Thermo Fisher Scientific), following the manufacturer's instruction. Data are expressed as a percentage of control after correction for protein content, determined using Bradford Reagent (Bio-Rad).

2.13 | Measurement of extracellular ROS

After transfection, 80,000 cells/well seeded in 12-well plates were analyzed by measuring extracellular H_2O_2 in intact cells after 3 days, using Amplex Ultra Red (50 µM) and horseradish peroxidase (0.1 U/ml) (Thermo Fisher Scientific) in HBSS without phenol red, for 2 h. Fluorescence readings were made in duplicate in 96-well plates at Ex/Em 530/590 nm using 100 µl of medium and were expressed as a percentage of control.

2.14 | Autophagy (Cyto-ID) assays

The amount of autophagic vacuoles was measured using the Cyto-ID kit (Enzo Life Sciences Inc.). One day after transfection, cells were treated with chloroquine for 16 h, harvested with accutase, washed, and stained for 30 min with Cyto-ID dye, analyzed in a BD Accuri-CG-Plus flow-cytometer (BD Biosciences) and specific signals were quantified using FlowJo software version 10.4.2.

2.15 | Caspase-3 activity assays

One, 3, or 6 days after seeding 500,000 cells/p60-dish, cells were collected, and caspase-3 activity was analyzed after lysis in 0.5% Triton X-100, 5 mM Tris–HCl, pH 8.0, 20 mM EDTA. A reaction mixture containing 20 µg of protein extract and 20 µM caspase-3 substrate (Ac-DEVD-AMC, BD Biosciences) in 20 mM HEPES, pH 7.5, 10% glycerol, 2 mM dithiothreitol, was incubated for 2 h in the dark at 37°C. Fluorescence (Ex/Em 380/440 nm) was measured in the microplate reader Enspire. A unit of caspase-3 activity is the amount of enzyme producing an increase in 1 fluorescence unit. Data are presented as units of caspase-3 activity/h/mg of protein, determined using Bradford Reagent (Bio-Rad).

2.16 | Cell proliferation and viability analysis

For quantification of Ki67-positive cells, 15,000 cells were seeded in eight-well chambered slides, cultured for 1 or 3 days, before fixation with 4% paraformaldehyde in PBS for 15 min at room temperature, incubation with anti-Ki67 antibody (Abcam; 1:1,000 dilution) overnight at 4°C, washing with PBS, incubating with anti-rabbit Alexa488 for 1 h at room temperature, and then stained with DAPI and mounted with fluoromount-G. Ten random pictures were taken with a Nikon Eclipse-90i microscope (×20 objective) at the same exposure time, and total (DAPI-positive) and Ki67-positive cell numbers were quantified by ImageJ64 10.2.

Cell viability was evaluated after drug treatments, on 3000 cells/well seeded as described above, with increasing concentrations of metformin or temozolomide (TMZ; Sigma-Aldrich) added 24 h later, and cell culture for 24 h. After treating cells with 10 µl PrestoBlue Cell Viability Reagent (Thermo Fisher Scientific) for 2 h, fluorescence (Ex/Em 540/590 nm) was measured using an EnSpire reader. Relative fluorescence units from treated cells normalized against dimethyl-sulfoxide (DMSO)-treated control cells are expressed as a percentage of viable cells. Compound IC_{50} was estimated from dose–response curves and defined concentrations for metformin and TMZ co-treatment. Experiments were performed in triplicate and data are expressed as mean ± *SEM*.

2.17 | Cell death assays

Two days after gene silencing, adherent and floating dead cells were harvested using accutase, centrifuged at 1100 rpm for 5 min, and resuspended in a final volume of 300 µl of PBS, containing 0.5 µg/ml of propidium-iodide. The incorporation of propidium-iodide was quantified by fluorescence-activated cell sorter analysis in a BD Accuri-CG-Plus flow-cytometer (BD Biosciences). To determine cell death induced by metformin, TMZ, or their combination, 1×10^5 transfected cells were seeded in a six-well dish. After 24 h, the drugs were added, and after an additional 24 h, floating and adherent cells were resuspended in 100 µl of annexin-V (AV) binding buffer and incubated with 1.0 µl of FITC-conjugated AV (Biolegend) and 1.0 µl of 7-aminoactinomycin D (7-AAD; Thermo Fisher Scientific). Flow cytometer analysis was performed using standard procedures on CytoFLEX (Beckman Coulter). GBM cells marked only with AV or 7-AAD were used to calibrate the flow cytometer according to the manufacturer's recommendations. These assays were performed in triplicate and data were analyzed using the FlowJo software.

2.18 | Statistical analysis

Data were analyzed using Prism GraphPad v7.0. Mann–Whitney test evaluated two-group comparisons. When more than two groups were compared, one-way analysis of variance and multiple paired comparisons were conducted using Turkey's or Bonferroni's posttest method.

3 | RESULTS

3.1 | LKB1 is enriched in SOX2^{high}/NESTIN^{high}/GFAP^{low} areas of GBM tumors

Using the GlioVis data portal (Bowman et al., 2017), we analyzed two public databases: TCGA Research Network (McLendon et al., 2008) and Gravendeel (Gravendeel et al., 2009). We compared *LKB1/STK11* expression levels in the three main GBM subtypes (CL, MS, PN) versus other glioma types and non-tumoral tissue, and estimated correlations between expression levels of *LKB1/STK11* and GBM stemness genes (*SOX2* and *NESTIN*). The datasets of TCGA indicated lower *LKB1/STK11* expression in GBM relative to non-tumoral tissue; a statistically insignificant trend for relative *LKB1/STK11* increase in various brain tumors compared to non-tumoral samples was observed in the Gravendeel database (Figure S1a). Interrogation of the three subtypes in both datasets did not provide statistically significant differences on *LKB1/STK11* expression, yet median expression was lower in MS and PN, relative to CL tumors (Figure S1b). Analyzing three independent GBM transcriptomic experiments in TCGA and one in Gravendeel, we identified weak/moderate expression correlations (coefficients: 0.2–0.4) between *LKB1/STK11* and *SOX2*, and between *LKB1/STK11* and *NESTIN* mRNAs (Figure S1c). As a positive control, the correlation between expression of the two established GBM stemness genes, *SOX2* and *NESTIN*, gave comparable coefficients (~0.3) in three experiments and better coefficients (0.64) in the U133plus experiment (Figure S1c).

The mRNA-based analyses from patient cohorts suggested that monitoring LKB1 protein might be a more accurate proxy to the function of LKB1.

We used a TMA with human GBM, anaplastic astrocytoma, and non-tumoral brain samples, and performed multiparametric immunohistochemistry for LKB1, SOX2, NESTIN, and the astrocytic marker GFAP (glial fibrillary acidic protein; Figure 1 and S2). Specific cells in every GBM sample showed high expression of LKB1, SOX2, and NESTIN, but almost undetectable levels of GFAP; we called these tumor cells SOX2^{high}/NESTIN^{high}/GFAP^{low} (Figures 1a and S2a). In contrast, tumor cells with high GFAP expression were almost devoid of LKB1 and NESTIN and had much lower SOX2 levels; we called these tumor cells SOX2^{low}/NESTIN^{low}/GFAP^{high} (Figures 1a and S2a). Non-tumoral brain sections revealed low expression of

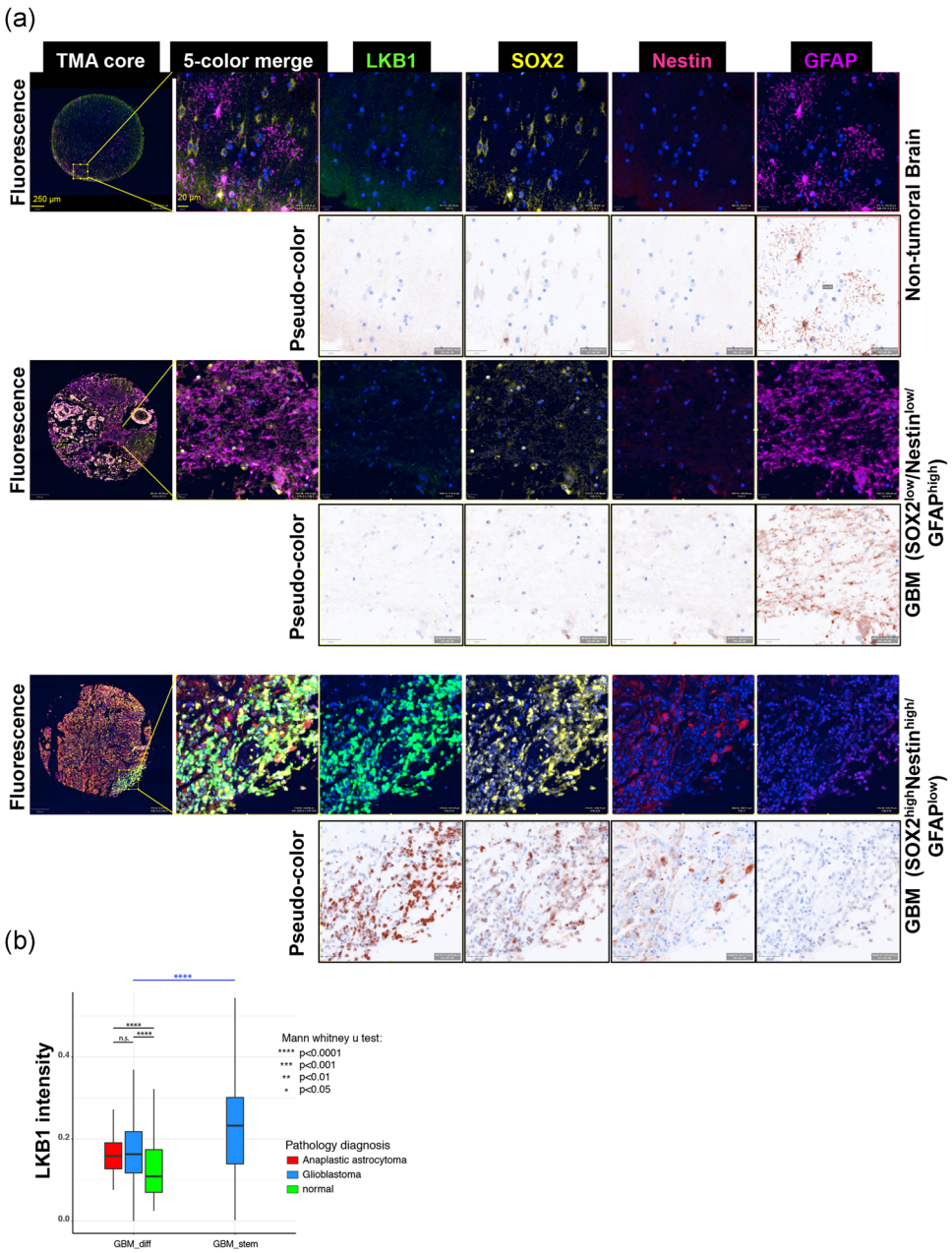

FIGURE 1 LKB1 protein analysis in GBM. (a) LKB1, SOX2, NESTIN, and GFAP immunolocalization in the non-tumoral brain and GBM tissue (representative images; Figure S2 shows more images). Original fluorescent images for the four different protein markers plus DAPI (blue), the 5-color merge, and the complete stained core are shown. The individual protein stainings are converted to brown pseudo-color. Magnification bars: 250 and 20 µm. (b) Glioblastoma, anaplastic astrocytoma, and non-tumoral brain tissue cells were classified into two groups, based on the expression of two different stem cell markers, NESTIN, and SOX2, and an astrocytic differentiation marker, GFAP: SOX2^{high}/NESTIN^{high}/GFAP^{low} (GBM_stem) and SOX2^{low}/NESTIN^{low}/GFAP^{high} (GBM_diff). Note that the GBM_stem group can only be identified in GBM (blue plot) but not in non-tumoral (normal, green plot) or anaplastic astrocytoma (red plot) tissues; significant differences at $^{****}p < 0.0001$. DAPI, 4′, 6-diamidino-2-phenylindole; GBM, glioblastoma; LKB1, liver kinase B1; n.s., not significant

LKB1, colocalizing with GFAP-positive astrocytes, the latter exhibiting their characteristic asteroid morphology (Figures 1a and S2a). For convenience in visual inspection, we converted each fluorescent channel to the same brown pseudo-color that resembles traditional immunohistochemical staining. We then quantified the number of cells expressing each protein and the number of fluorescent pixels per cell (Figure 1b). LKB1 protein "intensity" was compared between $SOX2^{high}/NESTIN^{high}/GFAP^{low}$ and $SOX2^{low}/NESTIN^{low}/GFAP^{high}$ cells. In Figure 1b, these groups are called GBM_diff (for differentiation that approximates non-tumoral brain signals) and GBM_stem (for GBM stem-like cells), respectively. Statistical analysis demonstrated that the non-tumoral brain ("normal" in Figure 1b) expressed the lowest median levels of LKB1 protein (green bar), with astrocytoma and GBM showing significantly higher expression (red and blue bars respectively). The $SOX2^{high}/NESTIN^{high}/GFAP^{low}$ (GBM_stem) cells expressed more LKB1 compared to the $SOX2^{low}/NESTIN^{low}/GFAP^{high}$ (GBM_diff) cells (Figure 1b). Pairwise protein staining analysis also showed that $GFAP^{high}$ astrocytes in nontumor brain expressed lower levels of LKB1 relative to $GFAP^{high}$ astrocytoma or GBM cells; the highest levels of LKB1 were recorded in the $GFAP^{low}$ GBM population (Figure S2b). Similarly, only low LKB1 levels could be detected in non-tumoral brain or even astrocytoma tissues characterized by $SOX2^{low}$ or $NESTIN^{low}$ cells (Figure S2b). Thus, LKB1 protein is expressed in GBM tumors, as predicted from the mRNA analysis (Figure S1), and is enriched in double-positive $SOX2^{high}$, $NESTIN^{high}$ cells, which potentially represent glioma stem-like cells. We, therefore, analyzed the contribution of LKB1 to the stem-like potential of patient-derived GBM cell cultures.

3.2 | LKB1 requirement for optimal gliomasphere formation

In agreement with the Gravendeel/TCGA analysis (Figure S1b), patient-derived cultures (U3005MG/PN, U3013MG/PN, U3017MG/CL, U3024MG/MS, U3028MG/CL, U3031MG/MS, U3034MG/MS), representing the three GBM subtypes (PN, CL, MS), expressed *LKB1* mRNA levels without statistically significant differences (Figure 2a). The two individual PN cultures expressed low LKB1 protein levels, one of the two CL cultures expressed undetectable LKB1 protein, and the second CL culture and two MS cultures exhibited higher (U3028MG, U3024MG, U3031MG) levels with one MS culture (U3034MG) expressing much lower levels of protein expression (Figure 2b). Thus, the variation in protein expression appeared independent of the GBM subtype. All cell cultures expressed robust levels of *NESTIN* and *SOX2* mRNA, whereas *GFAP* mRNA was high in the two CL and only in one MS culture (Figure 2a). The mRNA profiles mirrored relatively well the corresponding protein levels of NESTIN, SOX2, and GFAP, with the exception of U3017MG cells (Figure 2b).

We performed extreme limiting dilution assays (Hu & Smyth, 2009) and gliomasphere enumeration after culture in defined stem cell medium of the three independent 3D cultures, U3028MG/CL, U3031MG/MS, and U3034MG/MS (Figure 2c–e), the first two that reproducibly expressed the highest LKB1 protein levels, and the latter that was MS yet expressed lower LKB1 levels (Figure 2b). Comparable gliomasphere numbers and frequencies were observed among the three GBM cultures (Figure 2c,d). However, U3034MG/MS cells that expressed lower LKB1 protein (Figure 2b), resulted in a lower number of gliomaspheres (Figure 2e). LKB1 silencing using a pool of siRNAs (Figure S3a) reduced significantly the frequency of gliomasphere formation (Figure 2c,d), in agreement with studies on normal hematopoietic stem cells where LKB1 was shown to maintain self-renewal (Gan et al., 2010; Gurumurthy et al., 2010; Nakada et al., 2010). The efficiency of LKB1 silencing was 90% or higher and persisted over time, even at 6–7 days posttransfection, when gliomasphere assays were scored (Figure S3b). After screening four individual siRNAs targeting LKB1 (Figure S3c,d), siLKB1#8 and #10 were selected for further ELDA in the above three cultures and in U3005MG/PN; reproducibly, all tested siRNAs reduced the frequency of gliomasphere formation (Figure S4).

Reduction of 3D-gliomasphere frequency induced by LKB1 silencing coincided with less proliferation measured by Ki67 staining of U3028MG/U3031MG cells cultured in 2D laminin-adherent conditions (Figure S5). As 3D-gliomasphere assays are used as surrogate tests of stemness in vitro, and since stem cell maintenance has been linked to autophagy (Boya et al., 2018), we analyzed autophagic vacuole numbers by flow cytometry and autophagic proteins by immunoblotting. Treatment with the lysosomotropic agent chloroquine served as control as chloroquine inhibits autophagy and causes accumulation of autophagosomes (Iwai-Kanai et al., 2008). In addition, we used bafilomycin-A1, a vacuolar ATPase inhibitor, which blocks autophagosome-lysosome fusion and also enriches autophagosomes (Iwai-Kanai et al., 2008). LKB1 silencing caused a slight increase in the amount of U3031MG autophagosomes, which was lower than that caused by chloroquine treatment (Figure S6a). We also analyzed LC3-II and p62 levels, as key markers of autophagosome accumulation (Bjørkøy et al., 2005). In agreement with the flow cytometry results (Figure S6a), LKB1 silencing caused a very weak accumulation of LC3-II and a modest decrease in p62 protein levels, whereas the positive control bafilomycin-A1 enhanced the levels of both proteins (Figure S6b). These data suggest that LKB1 reduction weakly inhibits autophagic flux in GBM cultures.

We examined whether the decrease in proliferation observed after LKB1 silencing might reflect cell death. LKB1 silencing did not induce apoptosis measured as propidium iodide-enriched cells coupled to caspase-3 activity and cleaved caspase-3 accumulation (Figure S6c–e). The data support the notion that LKB1 can mark GBM tumor tissue with potential stem-like cells (Figure 1) and contributes to the generation of 3D-gliomaspheres (Figure 2), but makes a minor contribution to autophagy or survival in these GBM cultures.

3.3 | LKB1 suppresses GBM cell invasion

Previous evidence established that *miR-451* silences the scaffolding partner MO25/CAB39 and suppresses GBM migration

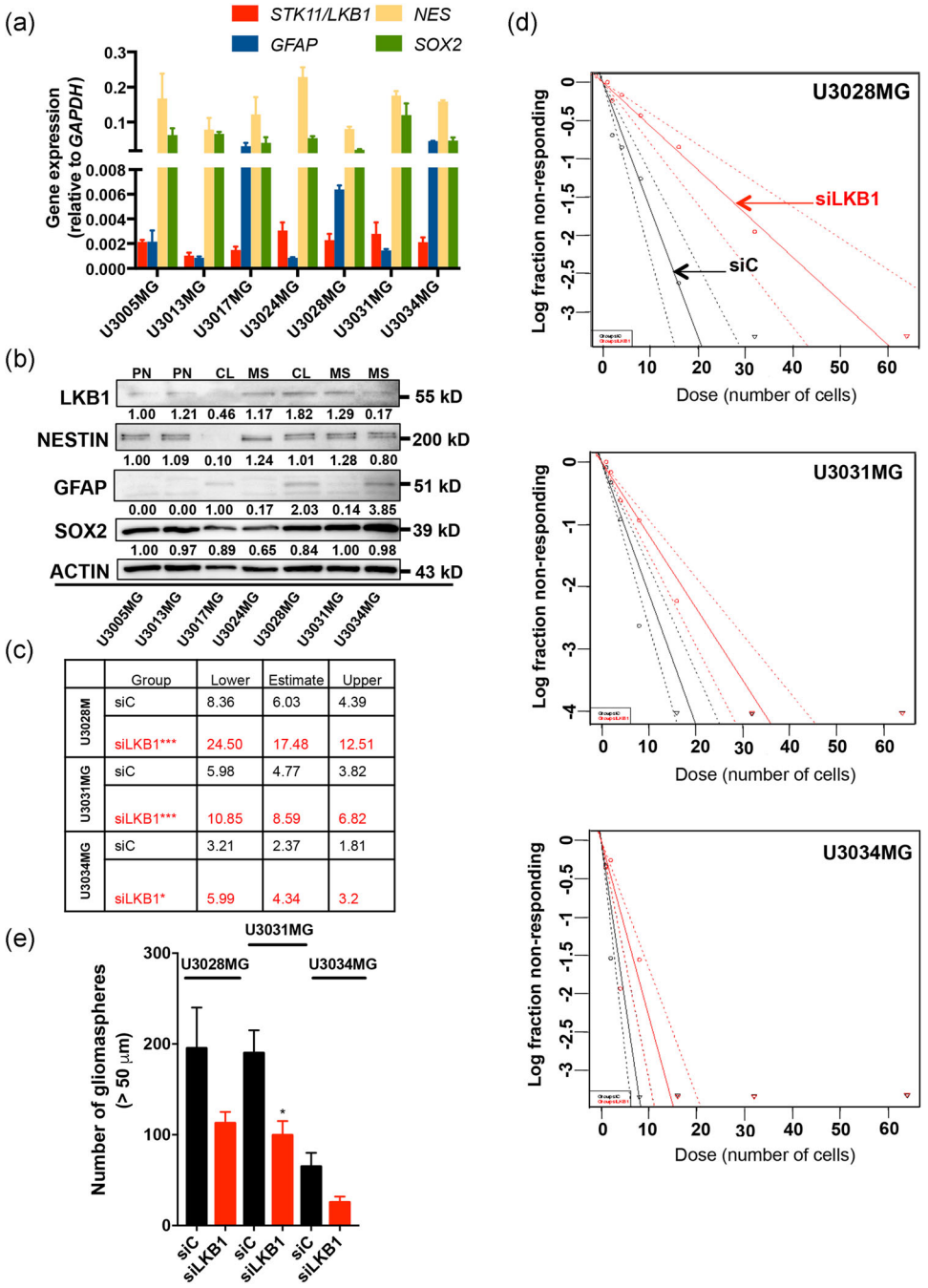

FIGURE 2 LKB1 is required for optimal gliomasphere formation. (a, b) RT-PCR (a) and immunoblot (b) analysis of LKB1/STK11, GFAP, NESTIN (NES), and SOX2 levels in GBM cultures; *GAPDH* served as a normalization control for mRNA and β-ACTIN (ACTIN) for protein analysis. Densitometric quantification of LKB1, NESTIN, GFAP, and SOX2 protein expression relative to β-ACTIN, with the basal expression level of each protein in U3005MG arbitrarily set to 1.00. Note the exception for GFAP, where the basal levels of U3017MG are expressed as 1.00. (c) Extreme limiting dilution assay table indicating average stem cell frequency per cell group (three to four independent experiments; seven technical repeats), and lower/upper confidence interval limits. (d) Extreme limiting dilution assay of three GBM cultures transfected with siC (black symbols) or siLKB1 (red symbols; siRNA pool) and cultured for 7 days. The number of sphere-containing wells per plating density is plotted. Steeper slopes indicate higher frequencies of sphere-forming cells. (e) Number of gliomaspheres (>50 μm) are shown as mean ± *SEM* of two independent experiments performed in duplicate, after transfection with siC (black bars) or siLKB1 (red bars; siRNA pool). Significant differences at $^{*}p < 0.05$, $^{***}p < 0.001$ by one-way analysis of variance. GAPDH, glyceraldehyde 3-phosphate dehydrogenase; GBM, glioblastoma; LKB1, liver kinase B1; mRNA, messenger RNA; RT-PCR, reverse-transcription polymerase chain reaction; siRNA, small interfering RNA

(Godlewski et al., 2010; Kim et al., 2011; Zhao et al., 2017), indirectly suggesting that LKB1 is required for tumor cell migration. By assessing the invasiveness of two mesenchymal (U3031MG and U3034MG) cultures across the physiological brain matrix laminin, we observed increased invasion upon LKB1 silencing (Figure 3a). The enhanced invasion observed in cultures was recapitulated in vivo when U3031MG cells were injected into the duct of Cuvier of zebrafish; U3031MG with silenced LKB1 extravasated from blood vessels and invaded the collagenous matrix of the fishtail more efficiently than control U3031MG cells (Figure 3b,c). The total number of injected fluorescent cells did not show significant variability between control and LKB1-silenced cell populations (Figure 3d). These results support the notion that LKB1 suppresses GBM cell invasion.

3.4 | Control of mitochondrial homeostasis by LKB1 in GBM

LKB1 gene deletion can deplete normal hematopoietic stem cells through impaired mitochondrial function and loss of metabolic energy (Gan et al., 2010; Gurumurthy et al., 2010; Nakada et al., 2010). We examined whether this occurs in the GBM cultures. LKB1 silencing induced an increase in intracellular (measured as 2,7-dichlorofluorescein diacetate [DCFH-DA] oxidation), but not extracellular ROS (Figures 4a,b and S7). Enhanced intracellular ROS generation after LKB1 silencing coincided with an increase in mitochondrial superoxide (measured as mitosox oxidation), a mild increase of mitochondrial membrane potential (measured using the mitotracker CMXROS reagent), and a concomitant reduction of

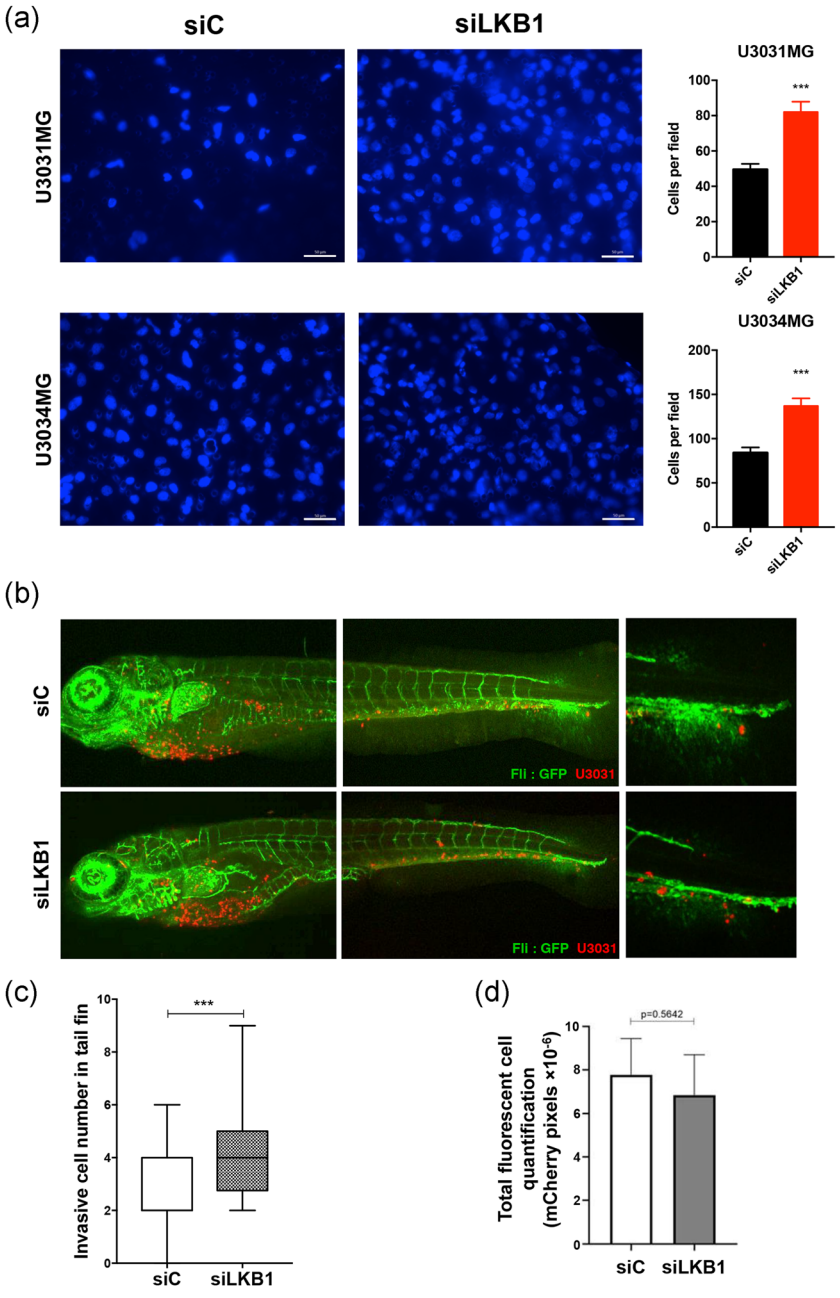

FIGURE 3 Silencing of LKB1 enhances GBM cell invasion. (a) U3031MG and U3034MG cells transfected with unspecific (siC) or LKB1-targeting (siLKB1 pool) siRNA were analyzed in invasion assays. Representative invading cell images (left, scale bar = 20 µm) and quantification of invading cells (right, $n = 3$ in duplicate; 20 fields quantified per independent experiment). (b) In vivo invasive capacity of U3031MG after silencing LKB1 (siLKB1 pool), assessed in zebrafish embryos. Representative images of circulating, invading GBM cells (red-marked cells) and vasculature (green due to endothelial-specific EGFP expression) in transgenic zebrafish are shown. Extravasation and collagenous tail fin invasion are observed (right-hand photomicrograph). Invading cells per fish, $n = 40$ were quantified, and presented as mean ± *SEM*. Statistical comparison (*t*-test); significant differences at $^{***}p < 0.001$. GBM, glioblastoma; LKB1, liver kinase B1; *SEM*, standard error of the mean; siRNA, small interfering RNA

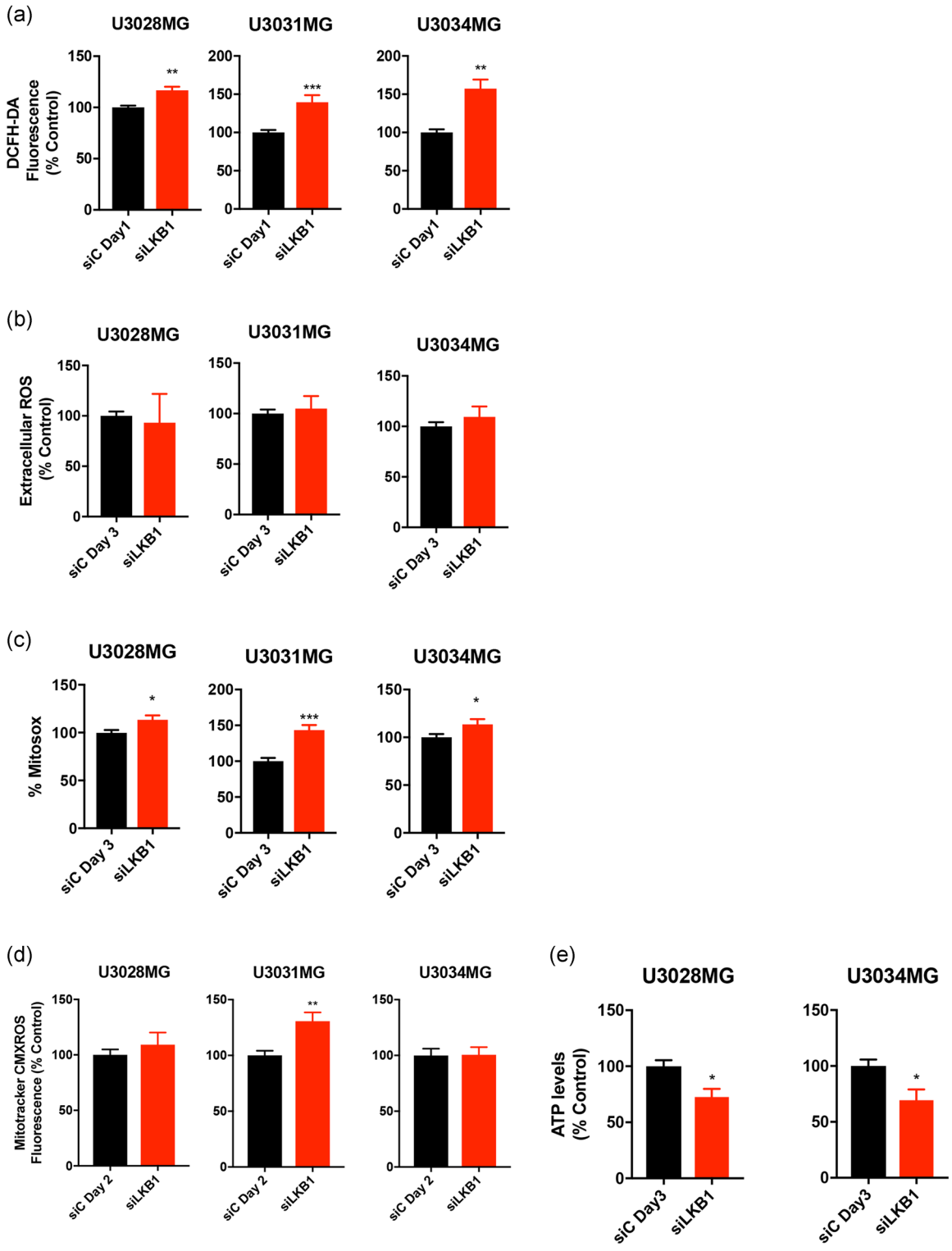

FIGURE 4 Silencing of LKB1 results in increased ROS production and reduced ATP levels. GBM cultures were transfected with siC (black bars) or siLKB1 siRNA (red bars; siRNA pool) for the indicated number of days. (a) Intracellular peroxide content was measured fluorimetrically using DCFH-DA; results are mean ± *SEM* of two to three independent experiments performed in triplicate. (b) Extracellular peroxide content was measured fluorimetrically using Amplex UltraRed; results are mean ± *SEM* of four independent experiments performed in quadruplicate. (c) Mitochondrial superoxide measured by MitoSOX Red; results are mean ± *SEM* of four to five independent experiments performed in triplicate. (d) Mitochondrial transmembrane potential by Mitotracker CMXROS; results are mean ± *SEM* of two to five independent experiments. (e) ATP levels; results are mean ± *SEM* of two independent experiments. A *t*-test indicates significant differences at: $^{*}p < 0.05$, $^{**}p < 0.01$, $^{***}p < 0.001$. DCFH-DA, 2,7-dichlorofluorescein diacetate; GBM, glioblastoma; LKB1, liver kinase B1; ROS, reactive oxygen species; *SEM*, standard error of the mean; siRNA, small interfering RNA

cellular ATP levels (Figure 4c–e). Thus, LKB1 can contribute to the homeostatic maintenance of mitochondrial metabolism in GBM cells.

3.5 | GBM cytotoxicity in response to metformin and temozolomide

LKB1 can activate AMPK family kinases as downstream effectors (Vaahtomeri & Mäkelä, 2011). Moreover, activation of AMPK by metformin, used for the treatment of type 2 diabetes, selectively kills GBM stem-like cells, demonstrated in gliomasphere assays (Carmignani et al., 2014). We, therefore, combined LKB1 silencing with metformin treatment (Figures 5 and S8). In U3031MG/MS and U3028MG/MS cells, metformin treatment activated endogenous phosphorylation of AMPKα (Figures 5a and S8a), as expected, and significantly reduced 3D-gliomasphere frequency in U3031MG cells (Figure 5b), in agreement with independent studies (Carmignani et al., 2014). In certain experiments with U3031MG cells, we observed that metformin treatment caused an increase in LKB1 protein levels (Figure 5a), an effect that was not reproduced in the U3028MG cells (Figure S8a). This may reflect a yet unknown signaling mechanism that has also been reported in pancreatic carcinoma cells (Song et al., 2018), which may not be universal. Silencing LKB1 exhibited a roughly 2-fold reduction in basal and metformin-induced phospho-AMPKα levels (Figures 5a and S8a). The negative effect of metformin on gliomasphere frequency was comparable but slightly stronger than the negative effect of LKB1 silencing; combining LKB1 silencing with metformin treatment resulted in greater gliomasphere reduction (Figure 5b). The metformin concentration used (5 mM) was slightly below the concentration exhibiting 50% toxicity (IC_{50}) (Figure S8b). Using higher metformin concentrations of 10 and 20 mM, we observed a weak apoptotic response based on increased cleavage of caspase-3 detection, which was enhanced after LKB1 silencing (Figure S8a, and see further below). Note, however, that the detection of cleaved caspase-3 is so low that precludes safe conclusions.

We also tested metformin in combination with the most widely used chemotherapeutic drug against adult GBM, temozolomide (Wen et al., 2020). TMZ exhibited IC_{50} values ranging from 180 ± 11.4 μM to 189 ± 9.3 μM in U3031MG and U3028MG cells, respectively (Figure S8c). Metformin and TMZ combination further decreased viability of the two GBM cultures and significantly reduced the TMZ IC_{50} values to 88.0 ± 5.1 μM in U3031MG and 70.4 ± 9.2 μM in U3028MG cells (Figures 5c–e and S8d-f). When LKB1 was silenced before treatment with the two drugs, no further change could be observed, confirming that depleting LKB1 phenocopied the action of metformin (Figures 5c–e and S8d–f). However, in U3028MG cells, LKB1 silencing reduced viability, independent of the dose of metformin (Figure S8e). To validate whether the observed cytotoxicity was due to the induction of cell death, the number of annexin-V^+ U3031MG cells was quantified by flow cytometry (Figures 5f and S9). LKB1 silencing or metformin treatment alone did not significantly increase the number of annexin-V^+ cells (Figure 5f), correlating to very weak cleavage of caspase-3 after metformin treatment alone (Figure S8a). Silencing LKB1 combined with metformin (10 and 20 mM) treatment enhanced caspase-3 cleavage (Figure S8a), however, this was not reflected in the annexin-V^+ cell assay (10 mM metformin; Figure 5f). LKB1 silencing promoted apoptosis of cells treated with TMZ either in the absence or presence of metformin (Figures 5f and S9). Thus, activating AMPK signaling by metformin enhances GBM cell killing by TMZ, which is independent of the presence or absence of LKB1. Loss of LKB1 can to some extent promote apoptosis under conditions of treatment with either metformin or TMZ.

3.6 | LKB1 regulates protein glycosylation-, EGF-, PDGF- and migration-related genes and suppresses stemness and cell cycle regulators in GBM

To explore pathways that possibly support the actions of LKB1 in GBM cells, we performed a transcriptomic analysis after silencing LKB1 in U3031MG and U3034MG. Using an adjusted p-value < 0.05 and −0.5<log FC>0.5, the 50 most significantly regulated genes for each culture were plotted in a heat-map (Figure S10a). Downregulation of 361 and 443 genes (Figure 6a) and upregulation of 206 and 304 genes (Figure S10b) in U3031MG and U3034MG, respectively, was observed. Using the gene set enrichment analysis web tool Enrichr (Kuleshov et al., 2016) and the R package clusterProfiler (Yu et al., 2012), we performed Gene Ontology Biological Process analysis of genes that were differentially regulated in both cell cultures. Silencing of LKB1 significantly downregulated genes classified under the GO terms of glycoprotein processing, EGF receptor signaling, and negative regulation of cellular response to growth stimuli, among others (Figure 6b,c), and upregulated genes related to neuronal and astrocytic differentiation (Figure S10c). Deeper analysis in the gene expression data of each separate cell culture, identified several oncogenic signaling factors (*AKT1*, *ELK1*, *ELK4*, *TEAD1*, *TEAD4*, *IGF2R*), a corresponding number of established stemness genes (*ALDH3A1*, *MYC*, *NOTCH1*, *NOTCH3*, *JAG1*, *WNT5B*, *WNT7B*, and a series of cell cycle regulators (*CDC25A*, *CDC25B*, *CCNA1*, *CCND1*, *CCND3*, *CCNE3*, *CDK1*) being mainly downregulated in at least one, and most frequently, in both cells, upon LKB1 silencing (Figure 6d). A more comprehensive list of such genes is presented in (Figure S11a). This is fully compatible with the requirement of LKB1 in stemness and proliferation assays (Figures 2, S4, and S5). The same gene analysis also indicated interesting genes that functionally associate with cell migration (Figure 6d). Cell surface adhesion and extracellular matrix genes that are known to resist cell detachment and migration were downregulated (*PODXL*, *TJP2*, *TIMP2*, *PDPN*, *CLDN11*), whereas genes that promote migration, including chemokines and matrix factors, were upregulated (*MMP1*, *CXCR4*, *FN1*, *COL1A2*, *CXCL5*, *HYAL1*) at least in one of the two cell models analyzed (Figure 6d). A more comprehensive list of such genes is presented in (Figure S11b). These results were further attested by a more unbiased GO analysis of downregulated genes in U3034MG

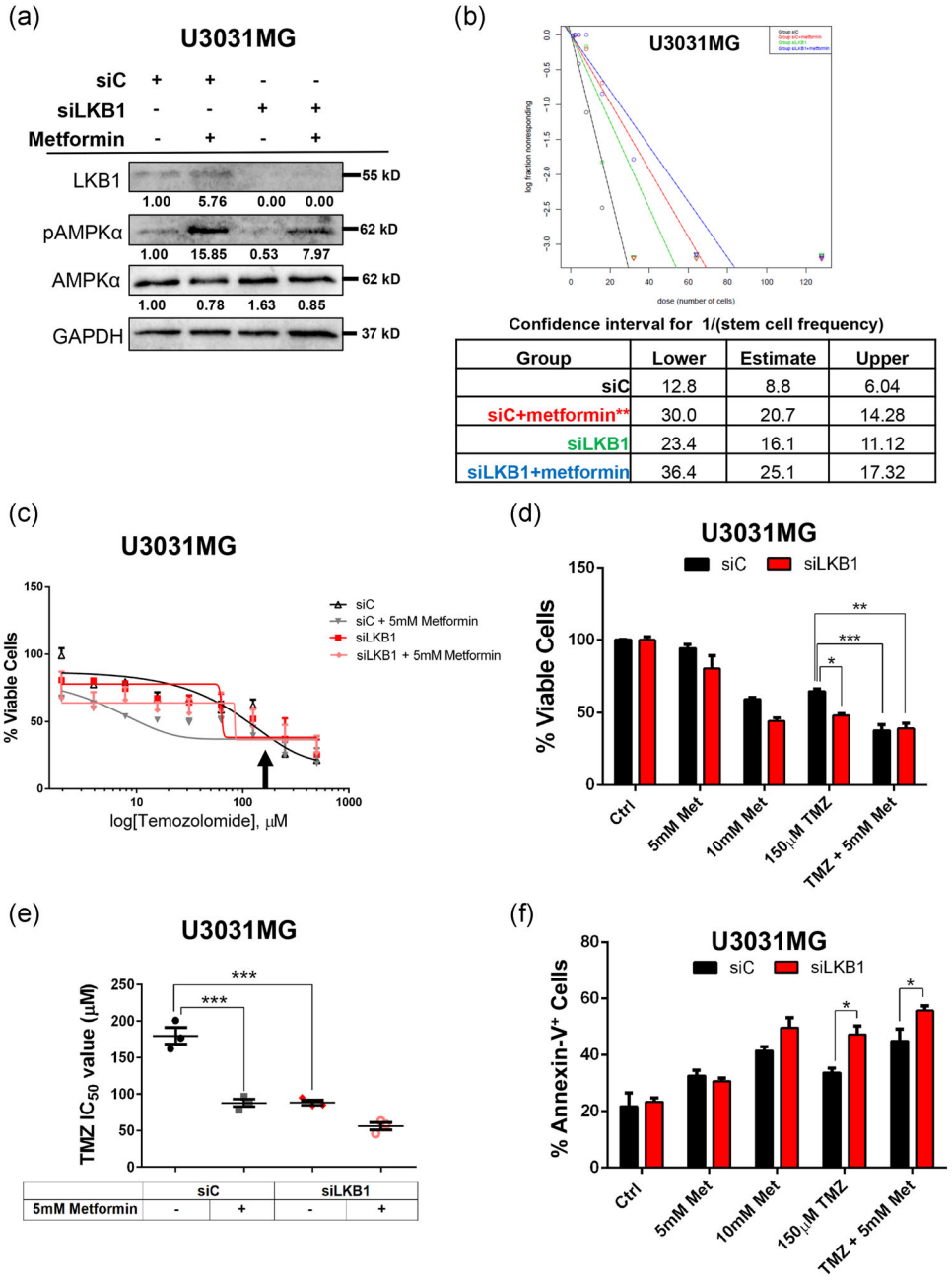

Group	Lower	Estimate	Upper
siC	12.8	8.8	6.04
siC+metformin**	30.0	20.7	14.28
siLKB1	23.4	16.1	11.12
siLKB1+metformin	36.4	25.1	17.32

FIGURE 5 Metformin- and temozolomide-mediated GBM cytotoxicity. (a) Efficiency of AMPKα activation by metformin. U3031MG cells were transfected with the indicated siRNAs for 48 h and treated with DMSO (-) or 5 mM metformin for another 24 h, before cell lysis and immunoblotting for the indicated proteins. Densitometric quantification of LKB1, phosphorylated (activation loop) AMPKα (pAMPKα) and total AMPKα protein levels relative to GAPDH, with the basal expression levels of LKB1, pAMPKα, and AMPKα in U3031MG siC (lane 1) arbitrarily set to 1.00. (b) Extreme limiting dilution assay of U3031MG cells transfected with siC (black, red symbols) or siLKB1 (green, blue symbols; siRNA pool), treated with DMSO (black, green symbols) or 5 mM metformin (red, blue symbols), and cultured for 7 days. The number of sphere-containing wells per plating density is plotted in the table below. (c) Cell viability assay of U3031MG cells transfected with siC or siLKB1, treated with DMSO, 5 mM metformin or increasing concentrations of TMZ, and cultured for 24 h. The % of viable cells is plotted relative to the siC treated only with DMSO. An arrow shows 125 μM TMZ used in panel (d). (d) Cell viability assay of U3031MG cells transfected with siC or siLKB1 (pool), treated with DMSO, 5 or 10 mM metformin with or without 125 μM TMZ, and cultured for 24 h. The percentage of viable cells is plotted relative to the siC treated only with DMSO. (e) The lowest dose of TMZ (μM) required for 50% inhibition of viability (IC_{50}) of U3031MG cells transfected with siC or siLKB1, co-treated with DMSO or 5 mM metformin and cultured for 24 h. (f) Cell death assay measuring the percent of annexin-V-positive cells using flow cytometry of U3031MG cells transfected with siC or siLKB1 (pool) and co-treated with DMSO, 5 or 10 mM metformin with or without 125 μM TMZ and cultured for 24 h. The results (b–f) are mean ± *SEM* of at least two independent experiments and significant differences at $^{*}p < 0.05$, $^{**}p < 0.01$ by one-way analysis of variance. GBM, glioblastoma; DMSO, dimethyl sulfoxide; GAPDH, glyceraldehyde 3-phosphate dehydrogenase; LKB1, liver kinase B1; siRNA, small interfering RNA; TMZ, temozolomide

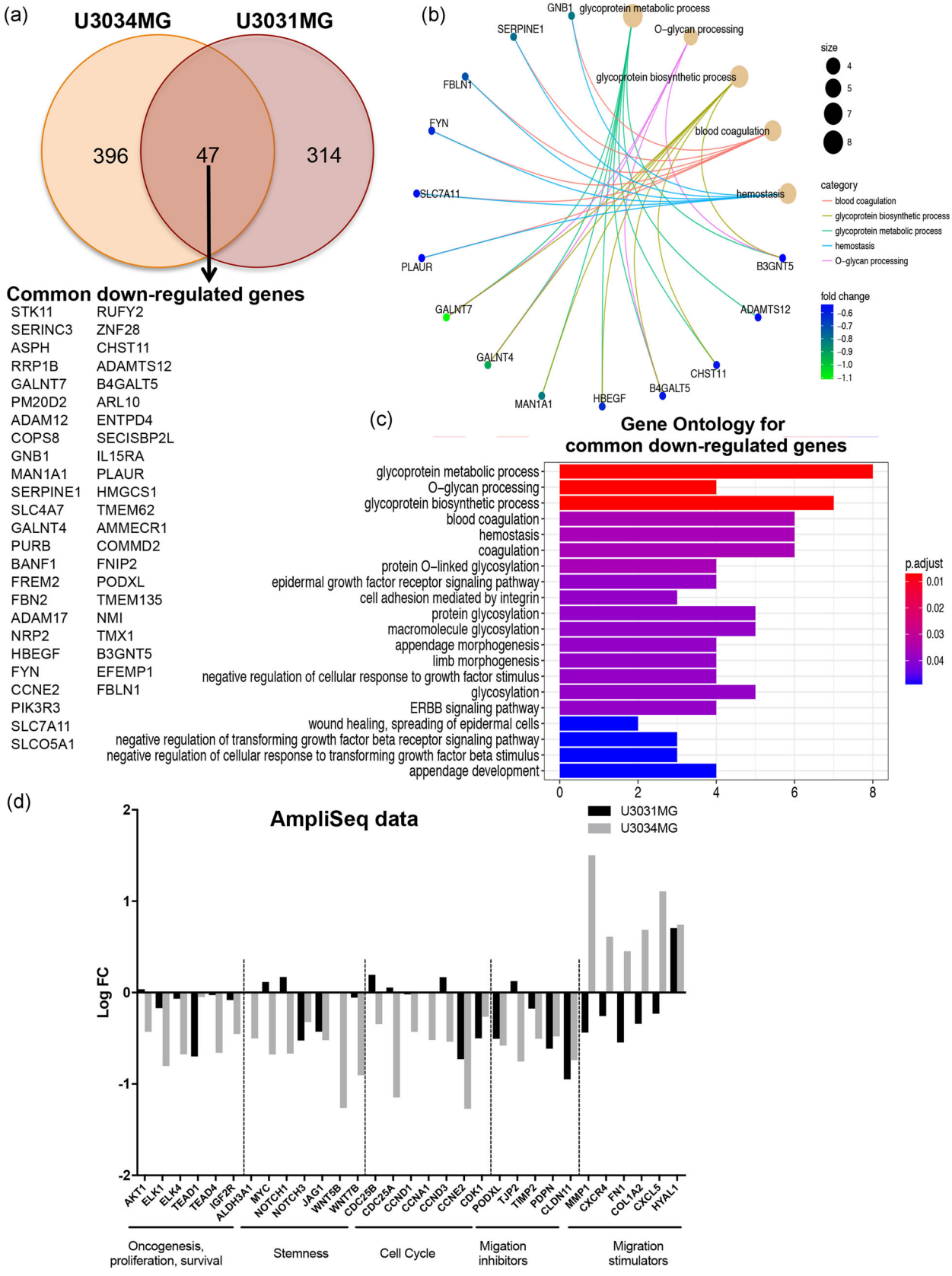

FIGURE 6 (See caption on next page)

and U3031MG cells (Figure S11c). Overall, these transcriptomic analyses suggested that the effect of LKB1 on gliomasphere formation and GBM invasiveness is multifactorial, yet they also pointed to a possible involvement of growth factor signaling.

Silencing of LKB1 repressed genes encoding EGF-like ligands, their receptors (Clark et al., 2012), and enzymes responsible for the shedding of EGF-like ligands from the plasma membrane (*ADAM10*, *ADAM17*), as well as genes encoding well-known inducers of GBM stem-like potential, such as the TGF-β isoforms, LIF (Ikushima et al., 2009; Peñuelas et al., 2009), PDGF isoforms and PDGF receptors (Cenciarelli et al., 2014; Dai et al., 2001) (Figure 7a). Based on the unbiased screen findings, we examined whether PDGF signaling could rescue the defect caused by LKB1 silencing. Addition of PDGF-BB, but not of PDGF-AA (not shown), rescued the decrease in gliomasphere frequency induced by LKB1 knock-down (Figure 7b,c; data not shown), suggesting that the observed reduction of GBM cell-derived PDGF-BB levels is biologically meaningful. However, investigation of transcriptional mechanisms of *PDGFB* expression under the control of LKB1 is warranted, as bioinformatic analysis of transcription factors that might link LKB1 activity to *PDGFB* gene regulation did not provide useful results (data not shown).

LKB1 silencing also reduced the expression of glial progenitor cell factors, *OLIG2* and *NESTIN*, a result from the unbiased screen that was reproduced using RT-qPCR (Figure 7d). Thus, LKB1 may be required to maintain expression of diverse genes (*PDGFs*, *OLIG2*, *NESTIN*) and through such a mechanism may support stem-like potential in GBM. The positive correlation between LKB1 and NESTIN expression observed in U3031MG cells (Figure 7d) corroborates the independent findings of enrichment of LKB1 in NESTIN-positive tumor cells (Figure 1).

4 | DISCUSSION

The function of LKB1 in GBM is far from understood. LKB1 is mutated in lung carcinomas and has established functions in epithelial tumorigenesis (Korsse et al., 2013; Vaahtomeri & Mäkelä, 2011). In GBM, LKB1 may either suppress tumor growth (Sobottka et al., 2000) or oncogenically promote proliferation and invasion (Godlewski et al., 2010; Kim et al., 2011; Zhao et al., 2017). Evaluating *LKB1* mRNA levels in public patient datasets did not reveal clear expression differences in GBM compared to other glioma subtypes or non-tumoral tissue (Figure S1). GBM shows high content in stem-like cells and high relapse rates (Alcantara Llaguno et al., 2016; Lathia et al., 2015). The patient TMA data that we analyzed revealed that LKB1 protein expression is enriched in GBM tumor cells that co-express SOX2 and NESTIN, and is relatively scarce in tumor cells enriched in GFAP protein expression (Figure 1). We suggest that quantitative multiparametric immunohistochemical analysis (Mezheyeuski et al., 2018) provides a useful tool for the screening of GBM and the generation of hypotheses based on molecular networks that can assist the selection of treatments for patients.

LKB1 maintains homeostasis of hematopoietic stem cells (Gan et al., 2010; Gurumurthy et al., 2010; Nakada et al., 2010) and sustains proliferation of leukemic stem cells (H. Wang, Sun, et al., 2017). In addition to the immunohistochemical analysis of GBM tumors (Figure 1 and S2), we provide new evidence that LKB1 positively contributes to GBM cell proliferation under stem cell growth conditions, as LKB1 silencing suppressed gliomasphere formation and lowered cell proliferation (Figures 2, S4, and S5). Independent studies suggested that lack of LKB1 may promote glioma cell proliferation (Yuan et al., 2019; K. Zhang et al., 2019). However, it is worth noting that the published experiments where LKB1 is genetically altered have largely relied on the established U87MG GBM cell line (Yuan et al., 2019; K. Zhang et al., 2019), which has recently been recommended to not be used for experiments with relevance to GBM oncology (Allen et al., 2016). The use of patient-derived GBM cultures grown in defined stem cell media in this study may explain the different results. Reduced gliomasphere growth can be explained in part by the fact that LKB1 silencing caused repression of key signaling pathways necessary for the survival of GBM stem-like cells (Wicher et al., 2012), including the PDGF, LIF, TGF-β, EGF, NOTCH, and WNT family ligands and receptors, and the ADAM family of proteases (Figures 6 and 7). In addition, suboptimal expression of these signaling factors may be responsible for the reduced levels of NESTIN and OLIG2, two important proteins for the maintenance of glial progenitor cells (Figure 7d). PDGF ligands and especially PDGF-BB have been demonstrated to support stemness in human GBM (Bruna et al., 2007; Jiang et al., 2011), which is consistent with our finding that addition of exogenous PDGF-BB fully rescued the gliomasphere defect caused by LKB1 silencing (Figure 7b,c). We interpret this result by considering an independent contribution/function of PDGF-BB signaling on top of the defective LKB1 background. However, it is possible that LKB1 might crosstalk with PFGF-BB signaling. Possible mechanisms of transcriptional regulation of the *PDGFB* gene by LKB1 signaling remain to be elucidated.

Lack of LKB1 in GBM cultures promoted invasion in vitro and in vivo (Figure 3), in agreement with evidence from several malignancies. In glioma (Yuan et al., 2019; K. Zhang et al., 2019) and breast cancer cells (Sengupta et al., 2017), loss of LKB1 promotes

FIGURE 6 Transcriptomic analysis of GBM cells after LKB1 knock-down. (a) Venn diagram and list showing common downregulated genes between U3031MG and U3034MG cells with a LogFC < −0.5 and FDR < 0.05. (b) Graphical representation of downregulated genes from the top GO BP terms (number of genes per category is shown by circle diameter; fold-change in expression by color). (c) Gene Ontology enrichment for BP of the 47 common downregulated genes after LKB1 silencing. Adjusted *p*-value is color-coded. (d) Graphical representation of the log-FC of the indicated genes (siLKB1 pool vs. siC from the Ampliseq analysis) derived from triplicate samples of the two GBM cultures. BP, biological process; FC, fold change; FDR, false discovery rate; GBM, glioblastoma; LKB1, liver kinase B1

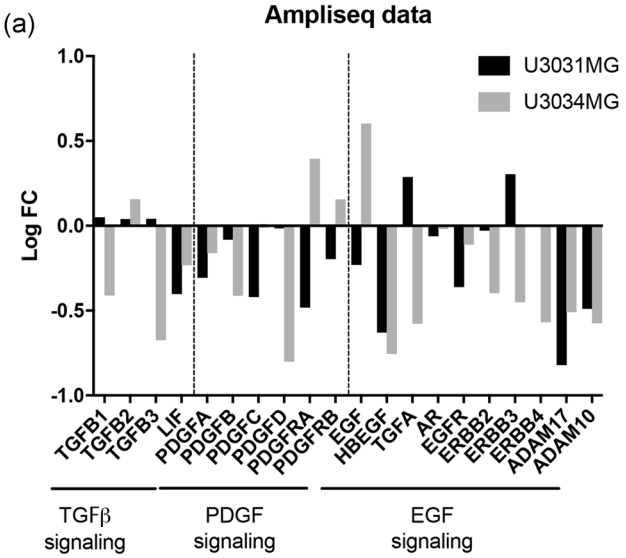

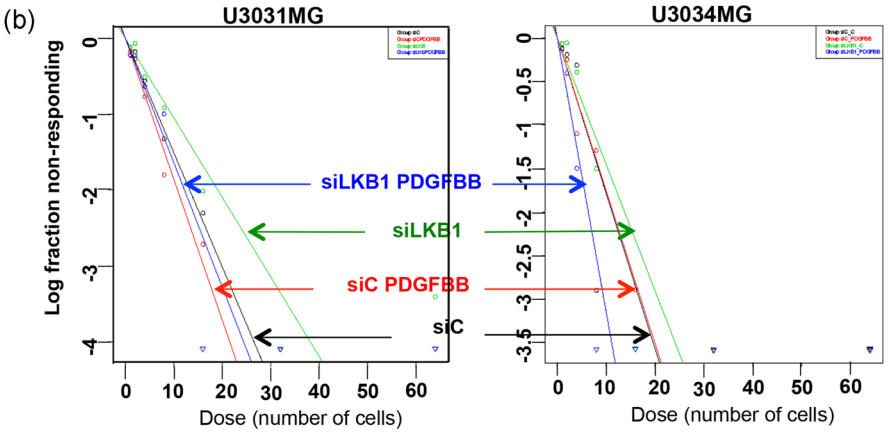

(c)

Confidence interval for 1/(stem cell frequency)

	Group	Lower	Estimate	Upper
U3031MG	siC	8.44	6.64	5.22
	siC PDGFBB	8.86	5.39	4.23
	siLKB1*	12.10	9.54	7.53
	siLKB1 PDGFBB**	7.66	6.10	4.80
U3034MG	siC	7.66	5.61	4.11
	siC PDGFBB	7.78	5.70	4.18
	siLKB1	9.39	6.89	5.06
	siLKB1 PDGFBB**	4.39	3.18	2.31

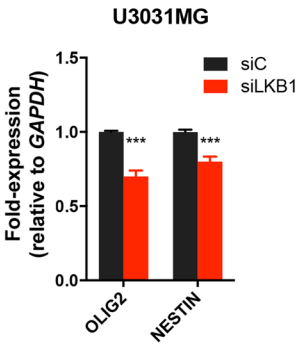

FIGURE 7 LKB1 maintains gliomasphere potential by regulating growth factor expression. (a) Graphical representation of the log-FC of the indicated genes (siLKB1 vs. siC Ampliseq analysis) derived from triplicate samples of the two GBM cultures. (b) Extreme limiting dilution assay of cells cultured in the indicated conditions (PDGF-BB 25 ng/ml). (c) The table indicates average stem cell frequency per cell group (three to four independent experiments; seven technical repeats), and lower/upper confidence interval limits. (d) Expression of the indicated genes after LKB1 silencing (pool); results are mean ± *SEM* of two independent experiments; significant differences as $^{*}p < 0.05$, $^{**}p < 0.01$, $^{***}p < 0.001$ by one-way analysis of variance. FC, fold change; GBM, glioblastoma; LKB1, liver kinase B1; PDGF, platelet-derived growth factor; *SEM*, standard error of the mean

invasiveness; in melanoma, loss of LKB1 expression cooperates with oncogenic BRAF/V600E to promote invasiveness (W. Zhang et al., 2017); and in ovarian cancer, overexpression of LKB1 represses invasiveness (Hong et al., 2017). So far, mechanistic evidence that links LKB1-mediated phosphorylation events to specific processes that regulate cancer cell motility is lacking. The closest approximation reported is inhibition of LKB1 kinase activity by the small molecule methylisoindigo in pancreatic ductal adenocarcinoma, which reduced the cancer stem cell population but also reduced carcinoma migration (Cheng et al., 2016). These findings agree with the reduced gliomasphere phenotype described here in GBM after silencing LKB1 (Figure 2), and contrast to our invasion results (Figure 3) and those from many cancer types (discussed above), possibly due to off-target effects of methylisoindigo.

Another direct mechanism involves the physical interaction between LKB1 and the adaptor protein nischarin, which associates with integrin receptors and suppresses a protein kinase-cofilin-dependent pathway that controls actin dynamics in breast cancer cells (Jain et al., 2013). A role for nischarin in GBM in association with LKB1 signaling would be interesting to examine in the future. Mechanisms established in glioma cells emphasized enhanced NF-κB signaling causing increased Snail1 expression, whose elevation was considered causative for the enhanced cell migration (Yuan et al., 2019). Similarly, LKB1 silencing in breast cancer cells induced expression of the transcription factor ZEB1, causing epithelial–mesenchymal transition and cancer cell invasiveness (Qiu et al., 2018). Indeed, Snail1 or ZEB1 overexpression in GBM increases invasiveness (Savary et al., 2013; Siebzehnrubl et al., 2013). Furthermore, Snail1 suppresses stem-like properties of GBM cells (Caja et al., 2018). We, therefore, hypothesized that silencing of LKB1 could impact Snail1, which could explain the two opposing effects, loss of stem-like potential and enhanced migratory ability. However, our efforts in this direction did not generate positive results. Snail1 was not upregulated in GBM cultures after LKB1 silencing neither were the Snail1-associated signaling pathways, that is, TGF-β isoforms, which were largely downregulated or not significantly changed (Figure 7a and File S2). In agreement with the above discussion, deeper inspection of the AmpliSeq analysis performed here (Figures 6, S10, and S11), demonstrated that silencing of LKB1 caused downregulation of several inhibitors of migratory behavior and upregulation of chemokines, chemokine receptors, and extracellular matrix proteins that usually assist cell migration. Thus, as GBM cells adapt to low expression of LKB1, a concomitant reorganization of matrix, cell surface receptors (including integrins), and chemokines that regulate cell motility takes place.

Furthermore, LKB1 silencing in GBM cells impaired the energetic output of mitochondria, resulting in increased mitochondrial-derived ROS and a corresponding reduction of ATP levels (Figures 6 and S7). Although the recorded changes led to the expectation that the GBM cells should exhibit a robust apoptotic response to the enhanced ROS and corresponding decreased ATP, these changes did not cause apoptosis and coincided with a weak impact on autophagy (Figure S6). The findings agree with studies in hematopoietic stem cells, where *LKB1* deletion resulted in mitochondrial dysfunction (Gan et al., 2010; Gurumurthy et al., 2010; Nakada et al., 2010). Mitochondrial misregulation provides an additional source for pro-migratory signals as ROS are well-established as central regulators of invasive potential in diverse tumors, including GBM (Singer et al., 2015). Thus, one possibility is that GBM cells with low LKB1 utilize their higher level of ROS for motility rather than undergoing programmed cell death.

LKB1 directly activates the AMPK family kinases, which promote glioma cell cycle inhibition and apoptosis (Strickland & Stoll, 2017). The AMPK pathway may act either positively or negatively in GBM development (Tang et al., 2016). Silencing of the chaperone HSP60 inhibits AMPK, and activates downstream mTOR signaling, reducing GBM cell proliferation, while enhancing invasion (Tang et al., 2016). GBM stem-like cells can exhibit low mTOR complex 1 kinase activity, mediating resistance to limited nutrition and maintenance of stemness (Han et al., 2017). Moreover, metformin, a clinically approved drug for the treatment of type 2 diabetes, activates AMPK signaling based on inhibition of the mitochondrial respiratory chain and depletion of ATP with a concomitant increase in AMP, the direct allosteric activator of AMPKs (Strickland & Stoll, 2017). In agreement with independent findings (Carmignani et al., 2014), treatment with metformin suppressed GBM gliomasphere formation, whereas inhibition of cell proliferation was observed only at metformin concentrations higher than 8 mM (Figures 5 and S8). These findings favor an anti-tumorigenic role for AMPK signaling. On the other hand, AMPK has been shown to promote cell cycle progression (Rios et al., 2013) and cell migration (Godlewski et al., 2010) in GBM. Furthermore, radiation and temozolomide-resistant human GBM stem-like cells exhibit increased AMPK phosphorylation (Strickland & Stoll, 2017). Influenced from these earlier studies (Wen et al., 2020), we also tested the impact of combination treatment with TMZ and metformin and recorded strongly negative effects on GBM culture viability (Figures 5 and S8). However, silencing of LKB1 had the same effect as metformin and did not rescue the enhanced sensitivity of GBM cells to the combinatorial treatment (Figure 5 and S8). Moreover, increased apoptosis was seen after LKB1 silencing only when the GBM cells were treated with TMZ, high metformin concentrations or their combination (Figures 5f and S8a). These observations agree with the established pathway that places AMPKs downstream of LKB1 and suggests that metformin and TMZ act independently.

Our data indicate that the presence of LKB1 contributes to enhanced GBM 3D-culture proliferation, limited mitochondrial activity, and limited invasive potential. These results underscore a dual role of LKB1 in GBM biology. Such dual roles, although abundantly described for many molecular regulators of tumor development, are often difficult to reconcile based on direct biochemical mechanisms. GBM stem-like potential is traditionally associated with enhanced invasiveness of the tumor (Alcantara Llaguno et al., 2016; Lathia et al., 2015). Thus, how can a protein kinase, like LKB1, support stem-like phenotypes and exhibit enrichment in NESTIN/SOX2-positive tumor cells, while also limiting the invasive potential of GBM cells? It is possible that the effect of LKB1 is context-dependent so that GBM cells with stem-like features may change their molecular pathways

when they generate migratory cells. Based on the cumulative results of this study, we suggest that as LKB1 mainly supports stem-like features of GBM cells, it counteracts the mechanisms that generate motility in the progeny of these cells. This speculative explanation will require careful fate mapping of GBM cells in the brains of mice where the migratory progeny can be distinguished from the pool of stem-like cells in which LKB1 has been genetically ablated or not. Alternatively, the availability of reliable LKB1 chemical inhibitors in the future may facilitate such studies. Our study, therefore, suggests caution, as treatment of GBM patients with LKB1 pathway inhibitors may provide certain advantages (e.g., TMZ-mediated cytotoxicity), or may unleash undesired tumor invasiveness.

ACKNOWLEDGMENTS

We thank Bengt Westermark, Lene Uhrbom, Karin Forsberg-Nilsson, and Patrick Micke (Department of Immunology, Genetics, and Pathology, Uppsala University, Sweden) for GBM cultures and access to the tumor immunohistochemistry facility, and members of our group, especially Mohamad M. Ali for technical assistance and discussions. AmpliSeq analysis was performed at the National Genomics Infrastructure Uppsala of the Science for Life Laboratory. The computations were performed on resources provided by SNIC through Uppsala Multidisciplinary Center for Advanced Computational Science. This study was funded by: Ludwig Cancer Research, Swedish Cancer Society (CAN 2015/438, CAN2018/469 to Aristidis Moustakas), Swedish Research Council (2014-3834, 2017-01588, 2018-02757 to Aristidis Moustakas, 2015-02757 and 2020-01291 to Carl-Henrik Heldin), European Research Council (787472 to Carl-Henrik Heldin), OE och Elda Johanssons stiftelse (2018, 2019), Petrus och Augusta Hedlunds Stiftelse (M2019-1065), Svenska Läkaresällskapets fonder (SLS-887701) and Magnus Bergvalls Stiftelse (2019-03444) to Laia Caja and Lisa Erikssons minnesfond (2013) to Laia Caja. The APC was funded by the Swedish Cancer Society CAN2018/469.

CONFLICT OF INTERESTS

The authors declare that there are no conflicts of interests.

AUTHOR CONTRIBUTIONS

Conceptualization: Laia Caja and Aristidis Moustakas; formal analysis: Laia Caja, Mahsa Shahidi Dadras, Artur Mezheyeuski, Dorival Mendes Rodrigues-Junior, Peter ten Dijke, Carl-Henrik Heldin, and Aristidis Moustakas; investigation: Laia Caja, Mahsa Shahidi Dadras, Artur Mezheyeuski, Dorival Mendes Rodrigues-Junior, Sijia Liu, Anna Taylor Webb, and Maria Catalina Gomez-Puerto; resources: Aristidis Moustakas; data curation: Laia Caja; writing—original draft preparation: Laia Caja; writing-review and editing: Laia Caja, Mahsa Shahidi Dadras, Carl-Henrik Heldin, and Aristidis Moustakas; visualization: Laia Caja; supervision: Aristidis Moustakas; project administration: Aristidis Moustakas; funding acquisition: Laia Caja, Aristidis Moustakas, Carl-Henrik Heldin. All authors have read and agreed to the published version of the manuscript.

ORCID

Aristidis Moustakas http://orcid.org/0000-0001-9131-3827

REFERENCES

Alcantara Llaguno, S. R., Xie, X., & Parada, L. F. (2016). Cell of origin and cancer stem cells in tumor suppressor mouse models of glioblastoma. *Cold Spring Harbor Symposia on Quantitative Biology*, *81*, 31–36. https://doi.org/10.1101/sqb.2016.81.030973

Allen, M., Bjerke, M., Edlund, H., Nelander, S., & Westermark, B. (2016). Origin of the U87MG glioma cell line: Good news and bad news. *Science Translational Medicine*, *8*(354), 354re3–354re3. https://doi.org/10.1126/SCITRANSLMED.AAF6853

Bao, S., Wu, Q., McLendon, R. E., Hao, Y., Shi, Q., Hjelmeland, A. B., Dewhirst, M. W., Bigner, D. D., & Rich, J. N. (2006). Glioma stem cells promote radioresistance by preferential activation of the DNA damage response. *Nature*, *444*(7120), 756–760. https://doi.org/10.1038/nature05236

Bjørkøy, G., Lamark, T., Brech, A., Outzen, H., Perander, M., Overvatn, A., Stenmark, H., & Johansen, T. (2005). p62/SQSTM1 forms protein aggregates degraded by autophagy and has a protective effect on huntingtin-induced cell death. *The Journal of Cell Biology*, *171*(4), 604–614. https://doi.org/10.1083/JCB.200507002

Bowman, R. L., Wang, Q., Carro, A., Verhaak, R. G. W., & Squatrito, M. (2017). GlioVis data portal for visualization and analysis of brain tumor expression datasets. *Neuro-Oncology*, *19*(1), 139–141. https://doi.org/10.1093/neuonc/now247

Boya, P., Codogno, P., & Rodriguez-Muela, N. (2018). Autophagy in stem cells: Repair, remodelling and metabolic reprogramming. *Development*, *145*(4), dev146506. https://doi.org/10.1242/dev.146506

Brennan, C. W., Verhaak, R. G., McKenna, A., Campos, B., Noushmehr, H., Salama, S. R., Zheng, S., Chakravarty, D., Sanborn, J. Z., Berman, S. H., Beroukhim, R., Bernard, B., Wu, C. J., Genovese, G., Shmulevich, I., Barnholtz-Sloan, J., Zou, L., Vegesna, R., Shukla, S. A., … TCGA Research, N. (2013). The somatic genomic landscape of glioblastoma. *Cell*, *155*(2), 462–477. https://doi.org/10.1016/j.cell.2013.09.034

Bruna, A., Darken, R. S., Rojo, F., Ocaña, A., Peñuelas, S., Arias, A., Paris, R., Tortosa, A., Mora, J., Baselga, J., & Seoane, J. (2007). High TGFβ-Smad activity confers poor prognosis in glioma patients and promotes cell proliferation depending on the methylation of the PDGF-B gene. *Cancer Cell*, *11*(2), 147–160. https://doi.org/10.1016/j.ccr.2006.11.023

Caja, L., Tzavlaki, K., Dadras, M. S., Tan, E.-J., Hatem, G., Maturi, N. P., Morén, A., Wik, L., Watanabe, Y., Savary, K., Kamali-Moghaddan, M., Uhrbom, L., Heldin, C. H., & Moustakas, A. (2018). Snail regulates BMP and TGFβ pathways to control the differentiation status of glioma-initiating cells. *Oncogene*, *37*(19), 2515–2531. https://doi.org/10.1038/S41388-018-0136-0

Carmignani, M., Volpe, A. R., Aldea, M., Soritau, O., Irimie, A., Florian, I. S., Tomuleasa, C., Baritchii, A., Petrushev, B., Crisan, G., & Valle, G. (2014). Glioblastoma stem cells: a new target for metformin and arsenic trioxide. *Journal of Biological Regulators and Homeostatic Agents*, *28*(1), 1–15. http://europepmc.org/abstract/MED/24750786

Cenciarelli, C., Marei, H. E., Zonfrillo, M., Pierimarchi, P., Paldino, E., Casalbore, P., Felsani, A., Vescovi, A. L., Maira, G., & Mangiola, A. (2014). PDGF receptor α inhibition induces apoptosis in glioblastoma cancer stem cells refractory to anti-Notch and anti-EGFR treatment. *Molecular Cancer*, *13*(1), 247. https://doi.org/10.1186/1476-4598-13-247

Chen, J., Li, Y., Yu, T.-S., Mckay, R. M., Burns, D. K., Kernie, S. G., & Parada, L. F. (2012). A restricted cell population propagates

glioblastoma growth following chemotherapy. *Nature*, *488*(7412), 522–526. https://doi.org/10.1038/nature11287

Cheng, X., Kim, J. Y., Ghafoory, S., Duvaci, T., Rafiee, R., Theobald, J., Alborzinia, H., Holenya, P., Fredebohm, J., Merz, K. H., Mehrabi, A., Hafezi, M., Saffari, A., Eisenbrand, G., Hoheisel, J. D., & Wölfl, S. (2016). Methylisoindigo preferentially kills cancer stem cells by interfering cell metabolism via inhibition of LKB1 and activation of AMPK in PDACs. *Molecular Oncology*, *10*(6), 806–824. https://doi.org/10.1016/j.molonc.2016.01.008

Clark, P. A., Iida, M., Treisman, D. M., Kalluri, H., Ezhilan, S., Zorniak, M., Wheeler, D. L., & Kuo, J. S. (2012). Activation of multiple ERBB family receptors mediates glioblastoma cancer stem-like cell resistance to EGFR-targeted inhibition. *Neoplasia*, *14*(5), 420–428. https://doi.org/10.1596/neo.12432

Dai, C., Celestino, J. C., Okada, Y., Louis, D. N., Fuller, G. N., & Holland, E. C. (2001). PDGF autocrine stimulation dedifferentiates cultured astrocytes and induces oligodendrogliomas and oligoastrocytomas from neural progenitors and astrocytes in vivo. *Genes & Development*, *15*(15), 1913–1925. https://doi.org/10.1101/gad.903001

Gan, B., Hu, J., Jiang, S., Liu, Y., Sahin, E., Zhuang, L., Fletcher-Sananikone, E., Colla, S., Wang, Y. A., Chin, L., & Depinho, R. A. (2010). Lkb1 regulates quiescence and metabolic homeostasis of haematopoietic stem cells. *Nature*, *468*(7324), 701–704. https://doi.org/10.1038/nature09595

Godlewski, J., Nowicki, M. O., Bronisz, A., Nuovo, G., Palatini, J., De Lay, M., Van Brocklyn, J., Ostrowski, M. C., Chiocca, E. A., & Lawler, S. E. (2010). MicroRNA-451 regulates LKB1/AMPK signaling and allows adaptation to metabolic stress in glioma cells. *Molecular Cell*, *37*(5), 620–632. https://doi.org/10.1016/j.molcel.2010.02.018

Gravendeel, L. A. M., Kouwenhoven, M. C. M., Gevaert, O., de Rooi, J. J., Stubbs, A. P., Duijm, J. E., Daemen, A., Bleeker, F. E., Bralten, L. B. C., Kloosterhof, N. K., De Moor, B., Eilers, P. H. C., van der Spek, P. J., Kros, J. M., Sillevis Smitt, P. A. E., van den Bent, M. J., & French, P. J. (2009). Intrinsic gene expression profiles of gliomas are a better predictor of survival than histology. *Cancer Research*, *69*(23), 9065–9072. https://doi.org/10.1158/0008-5472.CAN-09-2307

Gurumurthy, S., Xie, S. Z., Alagesan, B., Kim, J., Yusuf, R. Z., Saez, B., Tzatsos, A., Ozsolak, F., Milos, P., Ferrari, F., Park, P. J., Shirihai, O. S., Scadden, D. T., & Bardeesy, N. (2010). The Lkb1 metabolic sensor maintains haematopoietic stem cell survival. *Nature*, *468*(7324), 659–663. https://doi.org/10.1038/nature09572

Han, Y.-P., Enomoto, A., Shiraki, Y., Wang, S.-Q., Wang, X., Toyokuni, S., Asai, N., Ushida, K., Ara, H., Ohka, F., Wakabayashi, T., Ma, J., Natsume, A., & Takahashi, M. (2017). Significance of low mTORC1 activity in defining the characteristics of brain tumor stem cells. *Neuro-Oncology*, *19*, 636–647. https://doi.org/10.1093/neuonc/now237

Hong, B., Zhang, J., & Yang, W. (2017). Activation of the LKB1-SIK1 signaling pathway inhibits the TGF-β-mediated epithelial–mesenchymal transition and apoptosis resistance of ovarian carcinoma cells. *Molecular Medicine Reports*, *17*(2), 2837–2844. https://doi.org/10.3892/mmr.2017.8229

Hu, Y., & Smyth, G. K. (2009). ELDA: extreme limiting dilution analysis for comparing depleted and enriched populations in stem cell and other assays. *Journal of Immunological Methods*, *347*(1–2), 70–78. https://doi.org/10.1016/j.jim.2009.06.008

Huang, J., Chen, H., Wei, Q., Zhang, Z., Zhong, Z., & Xu, Y. (2017). Downregulation of LKB1 promotes tumor progression and predicts unfavorable prognosis in patients with glioma. *Oncology Letters*, *13*(3), 1688–1694. https://doi.org/10.3892/ol.2017.5631

Ikushima, H., Todo, T., Ino, Y., Takahashi, M., Miyazawa, K., & Miyazono, K. (2009). Autocrine TGF-β signaling maintains tumorigenicity of glioma-initiating cells through Sry-related HMG-box factors. *Cell Stem Cell*, *5*(5), 504–514. https://doi.org/10.1016/j.stem.2009.08.018

Iwai-Kanai, E., Yuan, H., Huang, C., Sayen, M., Perry-Garza, C., Kim, L., & Gottlieb, R. (2008). A method to measure cardiac autophagic flux in vivo. *Autophagy*, *4*(3), 322–329. https://doi.org/10.4161/AUTO.5603

Jain, P., Baranwal, S., Dong, S., Struckhoff, A. P., Worthylake, R. A., & Alahari, S. K. (2013). Integrin-binding protein nischarin interacts with tumor suppressor liver kinase B1 (LKB1) to regulate cell migration of breast epithelial cells. *Journal of Biological Chemistry*, *288*(22), 15495–15509. https://doi.org/10.1074/JBC.M112.418103

Jiang, Y., Boije, M., Westermark, B., & Uhrbom, L. (2011). PDGF-B can sustain self-renewal and tumorigenicity of experimental glioma-derived cancer-initiating cells by preventing oligodendrocyte differentiation. *Neoplasia*, *13*(6), 492–503. https://doi.org/10.1593/NEO.11314

Kim, Y., Roh, S., Lawler, S., Friedman, A., & Stemmer-Rachamimov, A. (2011). miR451 and AMPK mutual antagonism in glioma cell migration and proliferation: A mathematical model. *PLoS One*, *6*(12), e28293. https://doi.org/10.1371/journal.pone.0028293

Korsse, S. E., Peppelenbosch, M. P., & van Veelen, W. (2013). Targeting LKB1 signaling in cancer. *Biochimica et Biophysica Acta (BBA)—Reviews on Cancer*, *1835*(2), 194–210. https://doi.org/10.1016/j.bbcan.2012.12.006

Kuleshov, M. V., Jones, M. R., Rouillard, A. D., Fernandez, N. F., Duan, Q., Wang, Z., Koplev, S., Jenkins, S. L., Jagodnik, K. M., Lachmann, A., McDermott, M. G., Monteiro, C. D., Gundersen, G. W., & Ma'ayan, A. (2016). Enrichr: A comprehensive gene set enrichment analysis web server 2016 update. *Nucleic Acids Research*, *44*(W1), W90–W97. https://doi.org/10.1093/nar/gkw377

Lathia, J. D., Mack, S. C., Mulkearns-Hubert, E. E., Valentim, C. L. L., & Rich, J. N. (2015). Cancer stem cells in glioblastoma. *Genes & Development*, *29*(12), 1203–1217. https://doi.org/10.1101/gad.261982.115

McLendon, R., Friedman, A., Bigner, D., Van Meir, E. G., Brat, D. J., M. Mastrogianakis, G., & Thomson, E. (2008). Comprehensive genomic characterization defines human glioblastoma genes and core pathways, *Nature*, *455*(7216), 1061–1068. https://doi.org/10.1038/nature07385

Mezheyeuski, A., Bergsland, C. H., Backman, M., Djureinovic, D., Sjöblom, T., Bruun, J., & Micke, P. (2018). Multispectral imaging for quantitative and compartment-specific immune infiltrates reveals distinct immune profiles that classify lung cancer patients. *The Journal of Pathology*, *244*(4), 421–431. https://doi.org/10.1002/path.5026

Nakada, D., Saunders, T. L., & Morrison, S. J. (2010). Lkb1 regulates cell cycle and energy metabolism in haematopoietic stem cells. *Nature*, *468*(7324), 653–658. https://doi.org/10.1038/nature09571

Noushmehr, H., Weisenberger, D. J., Diefes, K., Phillips, H. S., Pujara, K., Berman, B. P., Pan, F., Pelloski, C. E., Sulman, E. P., Bhat, K. P., Verhaak, R. G., Hoadley, K. A., Hayes, D. N., Perou, C. M., Schmidt, H. K., Ding, L., Wilson, R. K., Van Den Berg, D., Shen, H., … Cancer Genome Atlas Research, N. (2010). Identification of a CpG island methylator phenotype that defines a distinct subgroup of glioma. *Cancer Cell*, *17*(5), 510–522. https://doi.org/10.1016/j.ccr.2010.03.017

Peñuelas, S., Anido, J., Prieto-Sánchez, R. M., Folch, G., Barba, I., Cuartas, I., García-Dorado, D., Poca, M. A., Sahuquillo, J., Baselga, J., & Seoane, J. (2009). TGF-β increases glioma-initiating cell self-renewal through the induction of LIF in human glioblastoma. *Cancer Cell*, *15*(4), 315–327. https://doi.org/10.1016/j.ccr.2009.02.011

Qiu, B., Wei, W., Zhu, J., Fu, G., & Lu, D. (2018). EMT induced by loss of LKB1 promotes migration and invasion of liver cancer cells through ZEB1-induced YAP signaling. *Oncology Letters*, *16*(5), 6465–6471. https://doi.org/10.3892/OL.2018.9445

R Core Team. (2017). *R: A language and environment for statistical computing, R Foundation for Statistical Computing, Vienna, Austria*.

Ren, J., Liu, S., Cui, C., & ten Dijke, P. (2017). Invasive behavior of human breast cancer cells in embryonic zebrafish. *Journal of Visualized Experiments*, *122*, 55459. https://doi.org/10.3791/55459

Rios, M., Foretz, M., Viollet, B., Prieto, A., Fraga, M., Costoya, J. A., & Senaris, R. (2013). AMPK activation by oncogenesis is required to maintain cancer cell proliferation in astrocytic tumors. *Cancer Research*, *73*(8), 2628–2638. https://doi.org/10.1158/0008-5472.CAN-12-0861

Ritland, S. R., Ganju, V., & Jenkins, D. R. B. (1995). Region-specific loss of heterozygosity on chromosome 19 is related to the morphologic type of human glioma. *Genes, Chromosomes and Cancer*, *12*(4), 277–282. https://doi.org/10.1002/gcc.2870120407

Robinson, M. D., McCarthy, D. J., & Smyth, G. K. (2010). edgeR: A bioconductor package for differential expression analysis of digital gene expression data. *Bioinformatics*, *26*(1), 139–140. https://doi.org/10.1093/bioinformatics/btp616

Savary, K., Caglayan, D., Caja, L., Tzavlaki, K., Bin Nayeem, S., Bergström, T., Jiang, Y., Uhrbom, L., Forsberg-Nilsson, K., Westermark, B., Heldin, C. H., Ferletta, M., & Moustakas, A. (2013). Snail depletes the tumorigenic potential of glioblastoma. *Oncogene*, *32*(47), 5409–5420. https://doi.org/10.1038/onc.2013.67

Schuetz, T. A., Becker, S., Mang, A., Toma, A., & Buzug, T. M. (2012). A computational multiscale model of glioblastoma growth: Regulation of cell migration and proliferation via microRNA-451, LKB1 and AMPK. *Conference proceedings: Annual international conference of the IEEE Engineering in Medicine and Biology Society. Annual conference*, *2012* (pp. 6620–6623). IEEE Engineering in Medicine and Biology Society. https://doi.org/10.1109/EMBC.2012.6347512

Sengupta, S., Nagalingam, A., Muniraj, N., Bonner, M. Y., Mistriotis, P., Afthinos, A., Kuppusamy, P., Lanoue, D., Cho, S., Korangath, P., Shriver, M., Begum, A., Merino, V. F., Huang, C. Y., Arbiser, J. L., Matsui, W., Győrffy, B., Konstantopoulos, K., Sukumar, S., … Sharma, D. (2017). Activation of tumor suppressor LKB1 by honokiol abrogates cancer stem-like phenotype in breast cancer via inhibition of oncogenic Stat3. *Oncogene*, *36*(41), 5709–5721. https://doi.org/10.1038/onc.2017.164

Siebzehnrubl, F. A., Silver, D. J., Tugertimur, B., Deleyrolle, L. P., Siebzehnrubl, D., Sarkisian, M. R., Devers, K. G., Yachnis, A. T., Kupper, M. D., Neal, D., Nabilsi, N. H., Kladde, M. P., Suslov, O., Brabletz, S., Brabletz, T., Reynolds, B. A., & Steindler, D. A. (2013). The ZEB1 pathway links glioblastoma initiation, invasion and chemoresistance. *EMBO Molecular Medicine*, *5*(8), 1196–1212. https://doi.org/10.1002/emmm.201302827

Singer, E., Judkins, J., Salomonis, N., Matlaf, L., Soteropoulos, P., McAllister, S., & Soroceanu, L. (2015). Reactive oxygen species-mediated therapeutic response and resistance in glioblastoma. *Cell Death & Disease*, *6*(1), e1601. https://doi.org/10.1038/cddis.2014.566

Singh, S. K., Hawkins, C., Clarke, I. D., Squire, J. A., Bayani, J., Hide, T., Henkelman, R. M., Cusimano, M. D., & Dirks, P. B. (2004). Identification of human brain tumour initiating cells. *Nature*, *432*(7015), 396–401. https://doi.org/10.1038/nature03128

Sobottka, S. B., Haase, M., Fitze, G., Hahn, M., Schackert, H. K., & Schackert, G. (2000). Frequent loss of heterozygosity at the 19p13.3 locus without LKB1/STK11 mutations in human carcinoma metastases to the brain. *Journal of Neuro-Oncology*, *49*(3), 187–195. https://doi.org/10.1023/A:1006442024874

Song, L., Guo, J., Chang, R., Peng, X., Li, J., Xu, X., Zhan, X., & Zhan, L. (2018). Lkb1 obliterates snail stability and inhibits pancreatic cancer metastasis in response to metformin treatment. *Cancer Science*, *109*, 1382–1392.

Strickland, M., & Stoll, E. A. (2017). Metabolic reprogramming in glioma. *Frontiers in Cell and Developmental Biology*, *5*, 43. https://doi.org/10.3389/fcell.2017.00043

Tang, H., Li, J., Liu, X., Wang, G., Luo, M., & Deng, H. (2016). Down-regulation of HSP60 suppresses the proliferation of glioblastoma cells via the ROS/AMPK/mTOR Pathway. *Scientific Reports*, *6*(1), 28388. https://doi.org/10.1038/srep28388

Team R. (2015). *RStudio: Integrated Development Environment for R*. RStudio Inc.

Vaahtomeri, K., & Mäkelä, T. P. (2011). Molecular mechanisms of tumor suppression by LKB1. *FEBS Letters*, *585*(7), 944–951. https://doi.org/10.1016/j.febslet.2010.12.034

Verhaak, R. G., Hoadley, K. A., Purdom, E., Wang, V., Qi, Y., Wilkerson, M. D., Miller, C. R., Ding, L., Golub, T., Mesirov, J. P., Alexe, G., Lawrence, M., O'Kelly, M., Tamayo, P., Weir, B. A., Gabriel, S., Winckler, W., Gupta, S., Jakkula, L., … Cancer Genome Atlas Research, N. (2010). Integrated genomic analysis identifies clinically relevant subtypes of glioblastoma characterized by abnormalities in PDGFRA, IDH1, EGFR, and NF1. *Cancer Cell*, *17*(1), 98–110. https://doi.org/10.1016/j.ccr.2009.12.020

Wang, H., Sun, R., Chi, Z., Li, S., & Hao, L. (2017). Live kinase B1 maintains $CD34^{+}CD38^{-}$ AML cell proliferation and self-renewal. *Molecular and Cellular Biochemistry*, *433*, 1–8. https://doi.org/10.1007/s11010-017-3032-y

Wang, Q., Hu, B., Hu, X., Kim, H., Squatrito, M., Scarpace, L., Decarvalho, A. C., Lyu, S., Li, P., Li, Y., Barthel, F., Cho, H. J., Lin, Y. H., Satani, N., Martinez-Ledesma, E., Zheng, S., Chang, E., Sauvé, C. G., Olar, A., … Verhaak, R. (2017). Tumor evolution of glioma-intrinsic gene expression subtypes associates with immunological changes in the microenvironment. *Cancer Cell*, *32*(1), 42–56.e6. https://doi.org/10.1016/j.ccell.2017.06.003

Wen, P. Y., Weller, M., Lee, E. Q., Alexander, B. M., Barnholtz-Sloan, J. S., Barthel, F. P., Batchelor, T. T., Bindra, R. S., Chang, S. M., Chiocca, E. A., Cloughesy, T. F., DeGroot, J. F., Galanis, E., Gilbert, M. R., Hegi, M. E., Horbinski, C., Huang, R. Y., Lassman, A. B., Le Rhun, E., … van den Bent, M. J. (2020). Glioblastoma in adults: A Society for Neuro-Oncology (SNO) and European Society of Neuro-Oncology (EANO) consensus review on current management and future directions. *Neuro-Oncology*, *22*(8), 1073–1113. https://doi.org/10.1093/neuonc/noaa106

Wicher, G., Holmqvist, K., & Forsberg-Nilsson, K. (2012). Common denominators of self-renewal and malignancy in neural stem cells and gliomaIn. R. Srivastava, & S. Shankar (Eds.), *Stem cells and human diseases* (pp. 387–418). Springer. https://doi.org/10.1007/978-94-007-2801-1_17

Xie, Y., Bergström, T., Jiang, Y., Johansson, P., Marinescu, V. D., Lindberg, N., Segerman, A., Wicher, G., Niklasson, M., Baskaran, S., Sreedharan, S., Everlien, I., Kastemar, M., Hermansson, A., Elfineh, L., Libard, S., Holland, E. C., Hesselager, G., Alafuzoff, I., … Uhrbom, L. (2015). The human glioblastoma cell culture resource: Validated cell models representing all molecular subtypes. *EBioMedicine*, *2*(10), 1351–1363. https://doi.org/10.1016/j.ebiom.2015.08.026

Yu, G., Wang, L. G., Han, Y., & He, Q. Y. (2012). ClusterProfiler: An R package for comparing biological themes among gene clusters. *OMICS: A Journal of Integrative Biology*, *16*(5), 284–287. https://doi.org/10.1089/omi.2011.0118

Yuan, Y., Li, S. L., Cao, Y. L., Li, J. J., & Wang, Q. P. (2019). LKB1 suppresses glioma cell invasion via NF-κB/snail signaling repression. *OncoTargets and Therapy*, *12*, 2451–2463. https://doi.org/10.2147/OTT.S193736

Zhang, K., Wang, J., Wang, J., Luh, F., Liu, X., Yang, L., Liu, Y. R., Su, L., Yang, Y. S., Chu, P., & Yen, Y. (2019). LKB1 deficiency promotes

proliferation and invasion of glioblastoma through activation of mTOR and focal adhesion kinase signaling pathways. *American Journal of Cancer Research*, *9*(8), 1650–1663. Retrieved from. http://www.ncbi.nlm.nih.gov/pubmed/31497348

Zhang, W., Yin, L., Song, G., Han, X., Yin, Z., & Luo, D. (2017). LKB1 loss cooperating with BRAF V600E promotes melanoma cell invasion and migration by up-regulation MMP-2 via PI3K/Akt/mTOR pathway. *Oncotarget*, *8*(69), 113847–113857. https://doi.org/10.18632/oncotarget.22943

Zhao, K., Wang, L., Li, T., Zhu, M., Zhang, C., Chen, L., Zhao, P., Zhou, H., Yu, S., & Yang, X. (2017). The role of miR-451 in the switching between proliferation and migration in malignant glioma cells: AMPK signaling, mTOR modulation and Rac1 activation required. *International Journal of Oncology*, *50*(6), 1989–1999. https://doi.org/10.3892/ijo.2017.3973

SUPPORTING INFORMATION

Additional Supporting Information may be found online in the supporting information tab for this article.

How to cite this article: Caja, L., Dadras, M. S., Mezheyeuski, A., Rodrigues-Junior, D. M., Liu, S., Webb, A. T., Gomez-Puerto, M. C., ten Dijke, P., Heldin, C.-H., & Moustakas, A. (2022). The protein kinase LKB1 promotes self-renewal and blocks invasiveness in glioblastoma. *J Cell Physiol*, 237, 743–762. https://doi.org/10.1002/jcp.30542